AMERICAN SOCIETY FOR MICROBIOLOGY | Journal of Virology®

CELLULAR RESPONSE TO INFECTION

HIV Replication and Latency in a Humanized NSG Mouse Model during Suppressive Oral Combinational Antiretroviral Therapy

Sangeetha Satheesan,[a,b]* Haitang Li,[b] John C. Burnett,[b]* Mayumi Takahashi,[b]* Shasha Li,[b]* Shiny Xiaqin Wu,[c] Timothy W. Synold,[d] John J. Rossi,[a,b] Jiehua Zhou[b]

[a]Irell and Manella Graduate School of Biological Sciences, Beckman Research Institute of City of Hope, Duarte, California, USA

[b]Department of Molecular and Cellular Biology, Beckman Research Institute of City of Hope, Duarte, California, USA

[c]Analytical Pharmacology Core Facility, Beckman Research Institute of City of Hope, Duarte, California, USA

[d]Department of Cancer Biology, Beckman Research Institute of City of Hope, Duarte, California, USA

ABSTRACT Although current combinatorial antiretroviral therapy (cART) is therapeutically effective in the majority of HIV patients, interruption of therapy can cause a rapid rebound in viremia, demonstrating the existence of a stable reservoir of latently infected cells. HIV latency is therefore considered a primary barrier to HIV eradication. Identifying, quantifying, and purging the HIV reservoir is crucial to effectively curing patients and relieving them from the lifelong requirement for therapy. Latently infected transformed cell models have been used to investigate HIV latency; however, these models cannot accurately represent the quiescent cellular environment of primary latently infected cells *in vivo*. For this reason, *in vivo* humanized murine models have been developed for screening antiviral agents, identifying latently infected T cells, and establishing treatment approaches for HIV research. Such models include humanized bone marrow/liver/thymus mice and SCID-hu-thy/liv mice, which are repopulated with human immune cells and implanted human tissues through laborious surgical manipulation. However, no one has utilized the human hematopoietic stem cell-engrafted NOD/SCID/IL2rγ^{null} (NSG) model (hu-NSG) for this purpose. Therefore, in the present study, we used the HIV-infected hu-NSG mouse to recapitulate the key aspects of HIV infection and pathogenesis *in vivo*. Moreover, we evaluated the ability of HIV-infected human cells isolated from HIV-infected hu-NSG mice on suppressive cART to act as a latent HIV reservoir. Our results demonstrate that the hu-NSG model is an effective surgery-free *in vivo* system in which to efficiently evaluate HIV replication, antiretroviral therapy, latency and persistence, and eradication interventions.

IMPORTANCE HIV can establish a stably integrated, nonproductive state of infection at the level of individual cells, known as HIV latency, which is considered a primary barrier to curing HIV. A complete understanding of the establishment and role of HIV latency *in vivo* would greatly enhance attempts to develop novel HIV purging strategies. An ideal animal model for this purpose should be easy to work with, should have a shortened disease course so that efficacy testing can be completed in a reasonable time, and should have immune correlates that are easily translatable to humans. We therefore describe a novel application of the hematopoietic stem cell-transplanted humanized NSG model for dynamically testing antiretroviral treatment, supporting HIV infection, establishing HIV latency *in vivo*. The hu-NSG model could be a facile alternative to humanized bone marrow/liver/thymus or SCID-hu-thy/liv mice in which laborious surgical manipulation and time-consuming human cell reconstitution is required.

Received 5 December 2017 **Accepted** 8 January 2018

Accepted manuscript posted online 17 January 2018

Citation Satheesan S, Li H, Burnett JC, Takahashi M, Li S, Wu SX, Synold TW, Rossi JJ, Zhou J. 2018. HIV replication and latency in a humanized NSG mouse model during suppressive oral combinational antiretroviral therapy. J Virol 92:e02118-17. https://doi.org/10.1128/JVI.02118-17.

Editor Guido Silvestri, Emory University

Address correspondence to John J. Rossi, jrossi@coh.org, or Jiehua Zhou, jzhou@coh.org.

* Present address: Sangeetha Satheesan, Comparative Medicine, Pfizer, La Jolla, California, USA; John C. Burnett, Center for Gene Therapy, Beckman Research Institute of City of Hope, Duarte, California, USA; Mayumi Takahashi, Center for Drug Evaluation and Research, U.S. Food and Drug Administration, Silver Spring, Maryland, USA; Shasha Li, Center for Gene Therapy, Beckman Research Institute of City of Hope, Duarte, California, USA.

KEYWORDS HIV latency and persistence, humanized NSG mouse model, oral antiretroviral therapy, combinatorial ART, suppressive HIV, humanized NSG mouse model

Combinatorial antiretroviral therapy (cART) can effectively suppress HIV load below the limit of detection. However, interruption of therapy causes a rebound in viremia (1). This demonstrates the existence of a stable reservoir of latently infected cells in which drug-resistant viruses may reside during long-term therapy and from which reactivated HIV-infected cells may emerge (2). Although multiple reservoirs have been proposed (3, 4), including several cell types and anatomical sites (e.g., central nervous system [CNS], lung, liver and lymphoid tissue), the largest latent HIV reservoir is resting memory $CD4^+$ T cells. These $CD4^+$ T cells can be subdivided into central memory T cells (T_{CM}: $CCR7^+$ $CD27^+$) and their derivatives, effector memory T cells (T_{EM}: $CCR7^-$ $CD27^-$), which form after TCR engagement (5), transitional memory T cells (T_{TM}) and terminal effector T cells (T_{TE}) (6). Due to the very small number of latently infected cells ($\sim$1 in 10^6 resting $CD4^+$ T cells) and a lack of distinctive surface markers, this latent reservoir has proven difficult to target for treatment (7, 8). Furthermore, the latent reservoir allows viruses to evade host immune responses or antiretroviral agents; latent reservoirs that are refractory to cART are considered the major contributor to rapid rebound, which can occur when latent cells become reactivated (9). As a result, cART cannot completely eradicate HIV and is often associated with unwanted side effects. HIV latency is therefore considered a primary barrier to HIV eradication, and purging the HIV reservoir is crucial to effectively curing patients and relieving them from the lifelong requirement for therapy (8).

A more complete understanding of the establishment and role of HIV latency would greatly enhance attempts to develop novel HIV purging strategies. Many studies of HIV latency have been performed using latently infected transformed cell lines (e.g., J-Lat cells, ACH2 cells), which possess various HIV proviruses and may contain one or more copies of the integrated provirus in different integration sites or epigenetic environments. However, cellular models of latency cannot accurately represent the quiescent cellular environment of primary latently infected cells that is found in HIV patients treated with suppressive cART, and experimental results often vary from one cell line to the next (4, 5). In this regard, primary human $CD4^+$ T cells are generally assumed to be superior to cell lines as an HIV-1 latency model. In addition, resting $CD4^+$ T cells isolated from cART-treated aviremic HIV-1-infected patients are the gold-standard tool for screening and evaluating antilatency drugs. Given that obtaining reservoir samples (e.g., primary $CD4^+$ cells and cells from the CNS) from human patients is challenging and involves restricted safety regulation and sophisticated technologies, *in vivo* humanized murine models provide versatile and crucial tools for the study of HIV biology, pathogenesis, and persistence (10). The major humanized mouse models currently used in HIV-1 research and their recent advances have been extensively discussed in several review articles (11–13).

In order to achieve durable reconstitution with human cells *in vivo*, so-called "humanization," we need to use immunodeficient recipient mouse strains that harbor various mutations (14), thus leading to defective immune function. For example, in severe combined immunodeficiency (SCID) mice (15), the mutation in the protein kinase, DNA-activated, catalytic polypeptide gene (*Prkdc*^{scid}) prevents the efficient DNA repair that plays an important role in T cell and B cell receptor rearrangement. In addition, in RAG-knockout mouse strains (16, 17), the recombination-activating genes *Rag1* and *Rag2* that are required in T cell and B cell receptor rearrangements are disrupted to inhibit adaptive immune response. However, these models have some drawbacks, such as increased susceptibility to radiation, production of unwanted T and B cells and relatively high levels of immune responses, therefore limiting their application in long-term HIV-1 research. By using SCID-humanized-thymus/liver mice (SCID-hu-thy/liv) in which human fetal thymus and liver tissue are implanted under the kidney

capsule, Brooks et al. demonstrated that HIV latency was readily established in thymocytes and that this process contributed to thymic and systemic HIV persistence in peripheral organs (18). However, the major limitation associated with the SCID-hu-thy/liv model is the low level of systemic human T cells and the low level of plasma viremia associated with infection of the thymic organoid. In this regard, through additional genetic modification, additional immunodeficient murine strains, such as NOD/SCID/IL2rγ^{null} (NSG), have been produced to support more efficient, long-term, stable, and systemic engraftment with human cells (19, 20). In NSG model, SCID mutation is combined with disruption of interleukin-2 (IL-2) receptor common γ chain (IL-2γg or IL-2γc), which interrupts critical cytokines signaling, thus reducing both adaptive and innate immune response (21). NSG newborn mice can be successfully reconstituted with human lymphoid and myeloerythroid components following the injection of human hematopoietic stem cell (HSCs) derived from fetal liver or umbilical cord blood or mobilized adult CD34$^+$ cells from peripheral blood. A wide variety of human cells, such as CD4$^+$ and CD8$^+$ T cells, NK cells, monocytes/macrophages, and dendritic cells, can be presented in multiple organs of the resulting hu-NSG mice, which allow the study of key adaptive immune responses and can be infected by HIV through multiple routes (22). The humanized bone marrow/liver/thymus (BLT) mouse model was also developed by transplantation of autologous human fetal liver CD34$^+$ cells into NSG mice that were previously implanted with thymus and liver tissues (23–25). In the BLT model, additional implantation of human liver/thymus tissue provides for the active education of human T cells, which allows more authentic human thymopoiesis (26). BLT mice therefore permit human HLA-restricted T cell responses in contrast to hu-NSG mice. BLT mice are susceptible to HIV infection and antiretroviral treatment. Moreover, the latently infected resting CD4$^+$ T cells (CD4$^+$ CD27$^+$ CCR7$^+$) are present in this model at levels comparable to those present in human patients undergoing antiretroviral treatment (27). However, although the BLT model is informative, it is only amenable to limited investigations, since it is produced via complicated surgical procedures (coimplantation of multiple tissue fragments under the kidney capsule) and with limited source material (thymus and liver tissue), yielding few model mice. Hu-NSG model proved to be a more flexible and surgery-free alternative of BLT model. It can generate some adaptive immune response and has been reported to support HIV replication and CD4$^+$ T cell depletion (22). However, no one has utilized the hu-NSG mouse model to systemically analyze the *in vivo* response to the oral cART regimen or HIV persistence and latency on suppressive cART.

In the present study, we therefore describe the application of the hu-NSG model for supporting HIV infection, testing oral administration of cART, and establishing HIV latency *in vivo*. We established the humanized NSG mouse model by transplanting human HSCs into NSG mice and then confirmed the presence of resting memory CD4$^+$ cells. We infected the mice with CCR5-tropic HIV and then orally administered the standard three-drug cART regimen in the drinking water. Our results showed a dramatic reduction in plasma viral load and a rebound in human CD4$^+$ T cell populations in the peripheral blood and key tissues. We observed that cART resulted in suppression of plasma viremia below the limit of detection. The discontinuation of cART resulted in a rapid viral rebound, suggesting the presence of persistent infection. Moreover, the animal model also allowed the recovery of resting CD4$^+$ T cells that expressed HIV only after *ex vivo* stimulation. HIV-infected human cells isolated from HIV-infected hu-NSG mice on suppressive cART acted as a latent HIV reservoir in lymphoid organs. Taken together, our results demonstrate that the *in vivo* hu-NSG model recapitulates several important aspects of HIV reservoirs in that it can dynamically support HIV replication, the response to antiretroviral treatment, and the establishment of viral latency.

RESULTS

HIV-susceptible human T cells and macrophages are presented in humanized NSG mice. We established humanized HSC-transplanted NOD/SCID/IL2γc^{null} (hu-NSG) mice that carry human CD4$^+$ T cells by engrafting neonatal NSG mice with human fetal

liver CD34$^+$ HSCs. At 8 to 12 weeks posttransplantation, we evaluated the engraftment of peripheral blood and various mouse tissues with human CD45$^+$ leukocytes using flow cytometry with anti-human CD45 antibody. Human CD45$^+$ cells were found in the peripheral blood and tissues, typically ranging from 20 to 80% of cells in the peripheral blood, 40 to 70% of cells in the spleen, 80 to 85% of cells in the bone marrow (Fig. 1A and see Fig. S1 in the supplemental material), >90% of cells in the thymus, and 5 to 15% of cells in the intestine (data not shown). Within the CD45$^+$ population, we evaluated specific hematopoietic lineages or immune subsets using flow cytometry with anti-human CD19, CD14, CD3, CD4, and CD8. A wide variety of human cells, such as CD4$^+$ and CD8$^+$ T cells, monocytes/macrophages, and B cells was observed in multiple organs of the resulting hu-NSG mice (Fig. 1B). Our results demonstrated that T cells (CD3$^+$ CD4$^+$ or CD3$^+$ CD8$^+$ subsets) and macrophages/monocytes (CD14$^+$ subsets) were present in the peripheral blood and the lymphoid organs (spleen). B cell progenitors (CD19$^+$ subsets) were detected in the bone marrow. Of particular interest was the presence of a large population of human CD4$^+$ CCR5$^+$ cells in the peripheral blood as shown previously (see Fig. S4E and F in reference 28), since these cells represent a significant population that is targeted by both HIV-1 in humans and SIV in primates.

To determine whether human lymphoid cells receive adequate signals to migrate to and repopulate murine lymphoid organs we harvested several lymphoid organs, including spleen, bone marrow, and the gastrointestinal (GI) and reproductive tracts of hu-NSG mice, at approximately 13 to 14 weeks posttransplantation. Histological analysis using anti-human CD45, CD4, and CD68 antibodies indicated an abundant accumulation of CD45$^+$ human cells that included various human immune cell subsets, particularly in the spleen and bone marrow (Fig. 1C). We observed both human CD4$^+$ T cell and macrophage subpopulations (CD4 and CD68 staining areas) in these organs. In the GI tract, the presence of immune aggregates was observed in both the small and the large intestine, with CD4$^+$ T cells and macrophages distributed within the intestinal crypts and intraepithelial within the villi, especially in the small intestine; in contrast, in the cecum, human cells were observed as isolated lymphoid follicles. These results demonstrate that the gut-associated lymphoid tissues of hu-NSG mice were reconstituted with human cells. This suggests that this model will be susceptible to mucosal HIV transmission, as has been demonstrated in humanized BLT mice (23). In the reproductive tract, the CD4$^+$ T cells and CD68$^+$ macrophages were diffusely distributed in the cervical-vaginal area, suggesting that this model may support HIV infection via vaginal exposure.

These data collectively confirmed the successful engraftment of NSG mice with human CD34$^+$ hematopoietic progenitor cells and their lineage-specific differentiation into HIV-susceptible human T cells and resident monocytes.

Hu-NSG mice are permissive to HIV infection. To determine the response of hu-NSG mice to HIV challenge, we injected mice intraperitoneally (i.p.) with HIV CCR5-tropic BaL virus (200 ng of p24 units). We drew blood samples at 2-week interval and separated the cellular and plasma fractions. We used quantitative reverse transcription-PCR (qRT-PCR) to detect the circulating cell-free virus (viral RNA [vRNA] copy numbers) in the plasma (Fig. 2A). We observed a rapid response to HIV challenge in which viral RNA copy numbers were dramatically increased from an average of 10^4 to 10^6/ml, indicating an established infection. As expected, no viral RNA was detected in uninfected control hu-NSG mice (data not shown). Loss of helper CD4$^+$ T cells is a hallmark of HIV infection during the acute stage of infection (9, 29). Thus, we conducted flow cytometry to measure CD4$^+$ T cells in the peripheral blood before and after infection. We observed a general pattern of decreased CD4$^+$ T cell counts after infection (Fig. 2B). Our data demonstrate that the viremic hu-NSG mice indeed recapitulate the major characteristics of HIV infection observed in human patients (30, 31).

HIV-1-infected hu-NSG mice dynamically respond to oral antiretroviral treatment. To evaluate the response of viremic hu-NSG mice to antiretroviral treatment, we

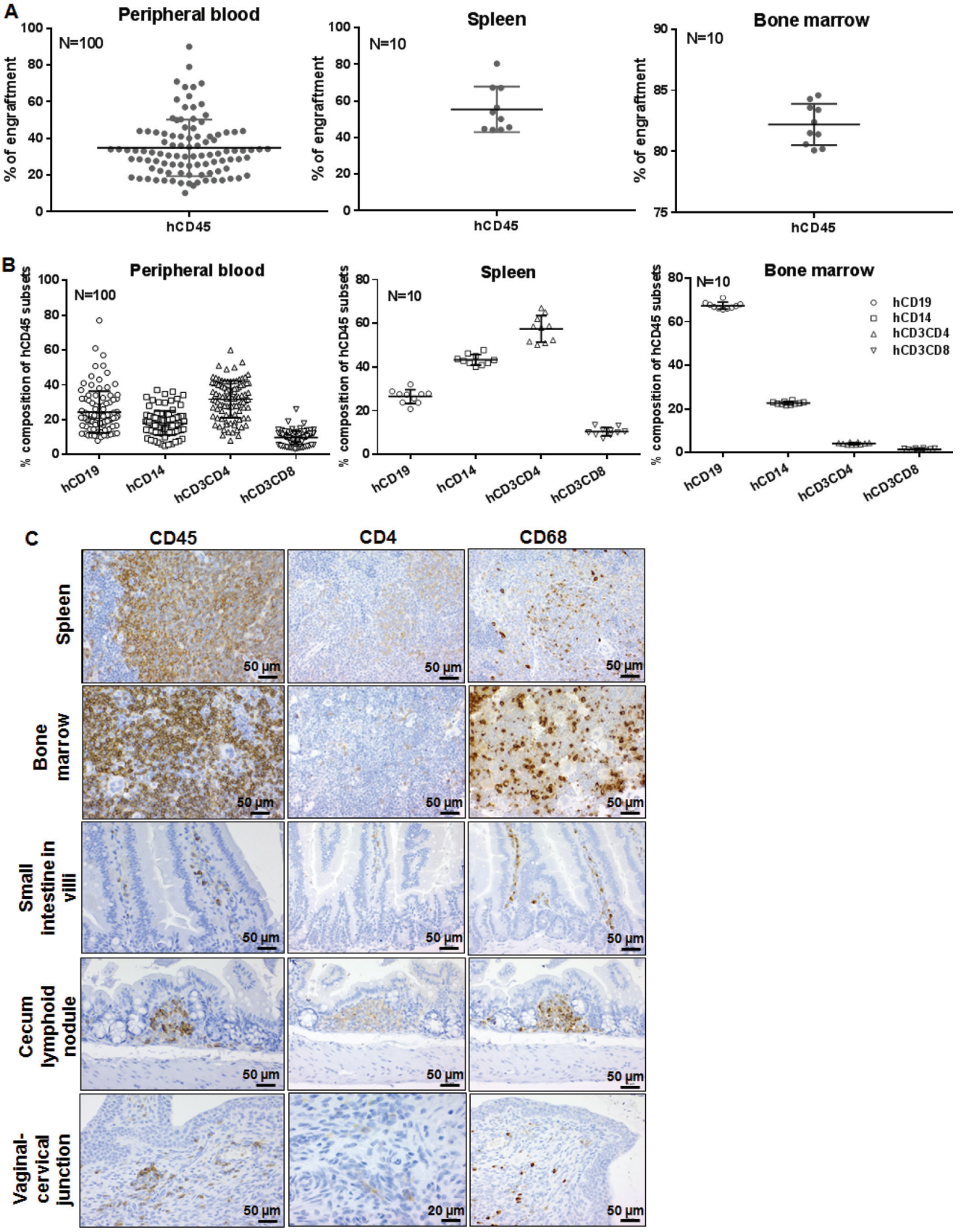

FIG 1 Establishment and evaluation of the hu-NSG mouse model. (A) Human CD45$^+$ cell population in peripheral blood, spleen, and bone marrow of NSG mice at 10 to 12 weeks posttransplantation with fetal-liver-derived CD34$^+$ HSCs. The graph shows the mean percentages of human CD45$^+$ cells measured

(Continued on next page)

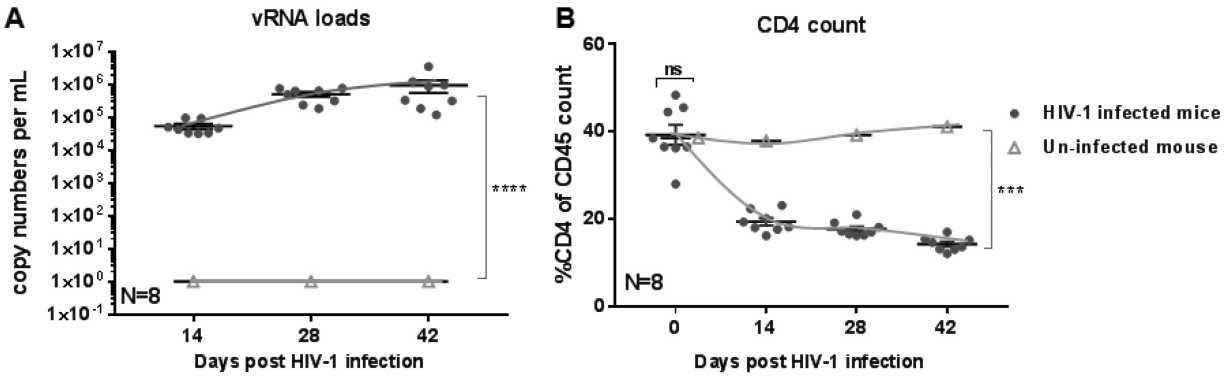

FIG 2 Response of hu-NSG mice to HIV infection. (A) Detection of plasma viremia in hu-NSG mice infected i.p. with CCR5-tropic HIV BaL virus. At the indicated days postinfection, blood samples were collected, and the plasma was analyzed by qRT-PCR for viral RNA. (B) Detection of $CD4^+$ T cell depletion in the peripheral blood of HIV-infected hu-NSG mice at the indicated days postinfection. Cells from blood samples that were stained with CD3 and CD4 antibodies were analyzed by flow cytometry. Prior to HIV-1 infection (day 0), the $CD4^+$ T cell population in peripheral blood was assayed by flow cytometry to obtain a baseline of $CD3^+$ $CD4^+$ T cell levels for each individual mouse. N, number of tested mice = 8; error bars, means ± the SEM. *, $P < 0.05$; **, $P < 0.01$; ***, $P < 0.001$; ****, $P < 0.0001$ (two-way analysis of variance [ANOVA]).

treated animals with three U.S. Food and Drug Administration (FDA)-approved therapeutic antiretroviral drugs (cART) that block new infections without inhibiting viral production in infected cells (tenofovir disoproxil fumarate [TDF], emtricitabine [FTC], and raltegravir [RAL]). We administered the three-drug cART regimen to viremic mice daily via drinking water formulation from 4 to 10 weeks postinfection (Fig. 3A). We monitored viral loads and $CD4^+$ T cell counts during treatment as described above. Viremic hu-NSG mice exhibited a robust suppression of viral load in response to the oral three-drug cART regimen within 2 weeks of treatment (day 42, closed circles, Fig. 3B), in contrast to control mice that did not receive cART (open triangles, Fig. 3B). This suppression persisted throughout the treatment period, and plasma viremia was suppressed to undetectable level within 4 weeks after initiation of cART (day 56, closed circles, Fig. 3B). At 2 and 4 weeks post-cART, $CD4^+$ T cell counts in the peripheral blood rebounded to levels similar to those observed before infection (days 42 and 56, closed circles, Fig. 3C); in contrast, $CD4^+$ T cell counts remained suppressed in control mice that did not receive cART (open triangles, Fig. 3C).

The CD4/CD8 ratio is a reflection of immune system health. It has been suggested as a frontier marker for clinical outcome and immune dysfunction in HIV-1 patients (32). An inverted CD4/CD8 ratio is characteristic of HIV-1 infection that significantly reduces a normal CD4/CD8 ratio between 1.5 and 2.5 to <1. In addition, ART initiation in the early phases of infection allows for greater recovery of the CD4/CD8 ratio (33). To determine the impact of HIV-1 infection and oral administration of cART on the CD4/CD8 ratio in the hu-NSG model, we measured $CD4^+$ T cell and $CD8^+$ T cells counts during treatment as described above. As shown in Fig. 3D, a normal CD4/CD8 ratio of 2.04 was observed before HIV-1 infection. However, a 3-week HIV-1 infection caused a depletion of $CD4^+$ T cells, consequently reducing the CD4/CD8 ratio to 0.59 (middle panel, Fig. 3D). Of note, at 4 weeks post-cART, $CD4^+$ T cells counts rebounds to normal level, and the CD4/CD8 ratio was recovered to >2 (right panel, Fig. 3D).

We further investigated the dynamic response of hu-NSG mice to cART disruption. After 6 weeks of treatment, we discontinued cART and monitored plasma viremia and $CD4^+$ T cell counts as described above. Viral rebound, defined as plasma viral RNA > 800 copies/ml,

FIG 1 Legend (Continued)
by flow cytometry. N, number of tested mice; error bars, means ± the SD. (B) Hematopoietic lineages or immune subsets within human $CD45^+$ cell population in peripheral blood, spleen, and bone marrow. The graph shows the mean percentages of various subsets, as indicated: $CD19^+$ (B cells), $CD14^+$ (monocytes/macrophages), and $CD3^+/CD4^+$ and $CD3^+/CD8^+$ (T cells) analyzed by flow cytometry. N, number of tested mice; error bars, means ± the SD. (C) Histological analysis of human immune cell engraftment in various lymphoid organs of hu-NSG mice, as indicated: spleen, bone marrow, intestinal tract (small intestine villi, cecum lymphoid nodule), and reproductive tract (vaginal-cervical junction). Tissue sections were subjected to immune staining with antibodies specific for human leukocytes ($CD45^+$), T cells ($CD4^+$), and macrophages ($CD68^+$), as indicated. Representative staining images are shown.

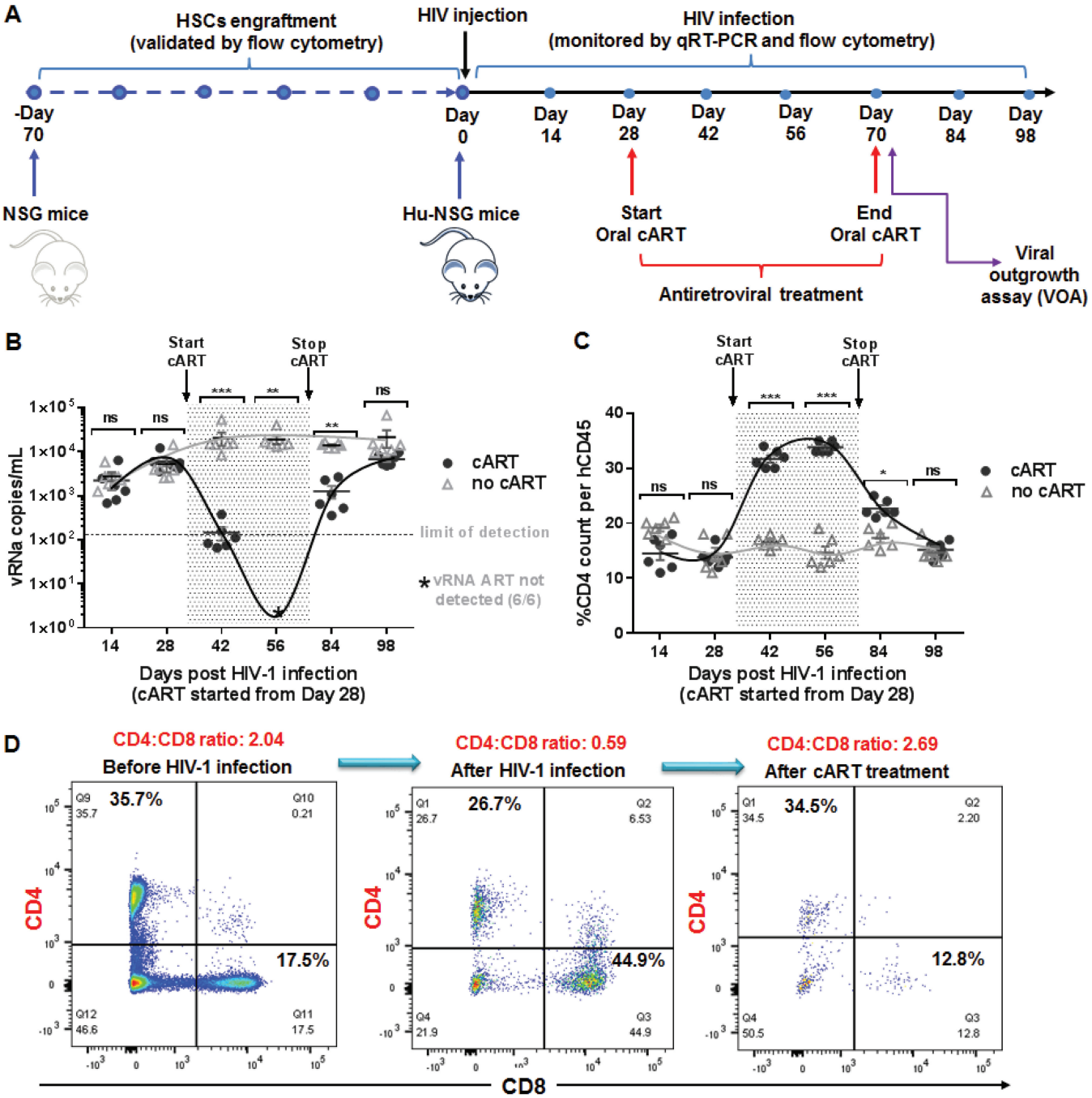

FIG 3 Dynamic response of HIV-infected hu-NSG mice to oral cART regimen. (A) Schematic of *in vivo* assessment of oral cART regimen in HIV-infected NSG mice. Hu-NSG mice were infected with HIV BaL. After confirmation of hu-NSG mice, cART drugs were orally administered for 6 weeks. At various days postinfection, blood samples were collected, and HIV infection progress was monitored by qRT-PCR (plasma viremia) and flow cytometry ($CD4^+$ T cell counts). (B) Detection of plasma viremia in the HIV-infected hu-NSG mice by qRT-PCR. The shaded area indicates the time period during which the mice received cART (from day 28 to day 70 as shown). The LOD (indicated by the dashed line) of the PCR assay is (ca. 110 to 160 RNA copies/ml) in 50 to 80 μl of plasma obtained through the tail vein. An asterisk (*) indicates that viral RNA was not detected in cART-treated animals at day 56. (C) Detection of $CD4^+$ T cell count by flow cytometry. N, number of tested mice = 6; error bars, means ± the SEM. *, $P < 0.05$; **, $P < 0.01$; ***, $P < 0.001$; ****, $P < 0.0001$; ns, no significant difference (two-way ANOVA). (D) Measurement of the CD4/CD8 ratio by flow cytometry. One representative flow graph is shown here to indicate the changes of CD4/CD8 ratio before and after HIV-1 infection and post-cART treatment.

was observed in all treated mice by 4 to 6 weeks after cART withdrawal (days 84 and 98, closed circles, Fig. 3B). As expected, $CD4^+$ T cells decreased quickly after the viral rebound and returned to levels similar to those before cART treatment or of untreated control mice (Fig. 3C). Our results suggest that a persistent viral reservoir was seeded

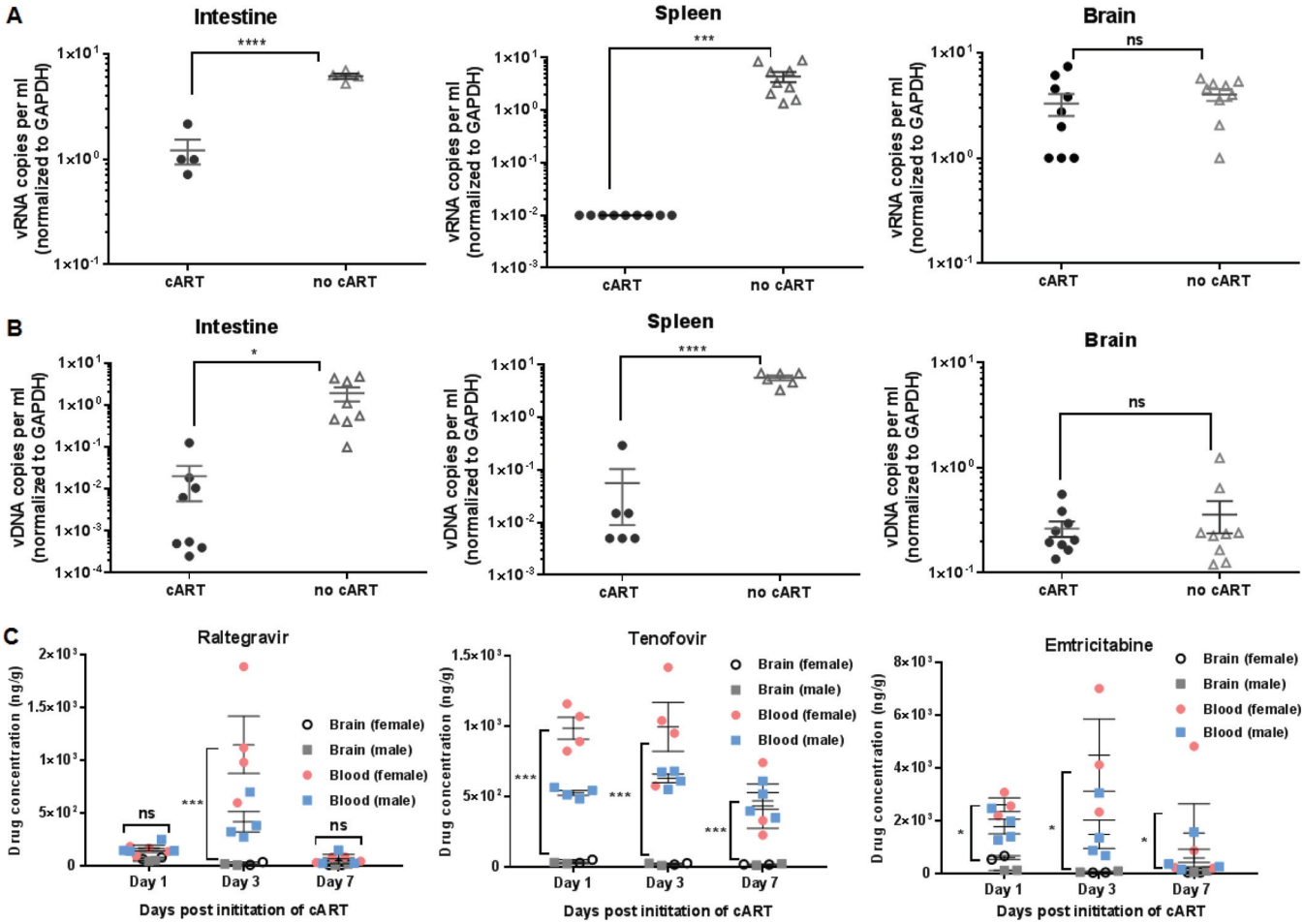

FIG 4 Effect of cART on residual vRNA and vDNA production in multiple tissues. (A) Detection of cell-associated vRNA levels in the intestines, spleens, and brains of HIV-infected hu-NSG mice on suppressive cART. (B) Detection of cell-associated vDNA levels in various tissues as described above. The vRNA or vDNA copy numbers in different tissues were normalized with the GAPDH gene. N, number of tested mice = 4 to 9; error bars, means ± the SEM. *, $P < 0.05$; **, $P < 0.01$; ***, $P < 0.001$; ****, $P < 0.0001$; ns, no significant difference (two-tailed Student *t* test analysis). (C) Drug quantification in mouse plasma in mouse brain. At different time points postinitiation of cART, the drug concentrations (raltegravir, tenofovir, and emtricitabine) in plasma in mouse peripheral blood or brain were determined by LC-MS. N, number of tested mice = 8 (4 female and 4 male). Data are presented as means ± the SD. *, $P < 0.05$; **, $P < 0.01$; ***, $P < 0.001$; ****, $P < 0.0001$; ns, no significant difference (one-way ANOVA).

in the hu-NSG mice after infection and subsequently led to viral rebound *in vivo* after cART discontinuation. Collectively, we demonstrated that oral administration of three-drug cART allows rapid suppression of plasma viremia and robust recovery of $CD4^+$ T cells in hu-NSG mice, analogous to the experience of cART-treated HIV-1-infected patients.

Oral antiretroviral treatment inhibits residual viral RNA and DNA production in the intestine and spleen, but not the brain. Humanized mouse models provide the unique ability to simultaneously examine multiple tissues throughout the course of cART, which is not possible in patients. To evaluate the impact of oral administration of cART on the production of viral RNA and viral DNA in multiple organs of hu-NSG mice on suppressive cART (day 70, Fig. 3A), we conducted qRT-PCR to measure cell-associated viral RNA (vRNA) and viral DNA (vDNA) levels in the GI tract, spleen, and brain. Compared to untreated control mice, we observed a decline in cell-associated vRNA levels after cART in the intestine and the spleen, but not in the brain (Fig. 4A). Similarly, the vDNA levels in the GI tract and spleen, but not in the brain, were dramatically reduced compared to the untreated mice (Fig. 4B). This is consistent with the observation that cART-treated individuals show a significant decrease in total HIV DNA proviral load in peripheral blood mononuclear cells (PBMCs) (34). The lack of suppression in the brain is probably due to less penetration of the drugs (Fig. 4C) (35).

A

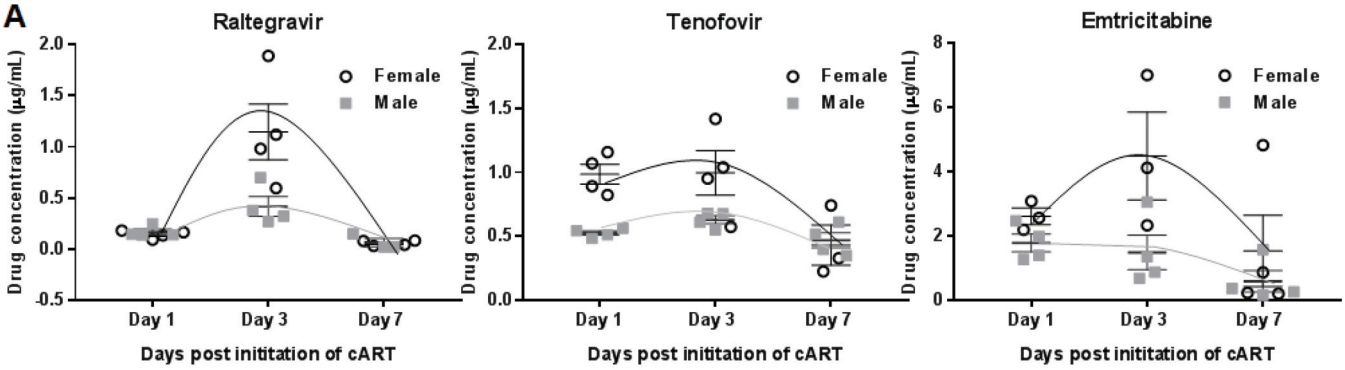

B

Antiretroviral drug	Subject	$C_{24\,h}$	$AUC_{0\text{-}24\,h}$	$C_{72\,h}$	$AUC_{0\text{-}72\,h}$
Raltegravir	Male mice	0.168 ± 0.039	4.02	0.418 ± 0.167	30.10
	Female mice	0.143 ± 0.028	3.44	1.147 ± 0.470	82.58
	human*	0.0395 - 0.399	9.5 - 13.4		
Tenofovir disoproxil fumarate	Male mice	0.527 ± 0.025	12.60	0.630 ± 0.053	45.36
	Female mice	0.987 ± 0.110	23.67	0.997 ± 0.300	71.78
	Human**	0.024 - 0.618	2.093 - 3.372		
Emtricitabine	Male mice	1.775 ± 0.484	42.60	1.486 ± 0.936	106.99
	Female mice	2.61 ± 0.365	62.64	4.49 ± 1.932	323.28
	human***	1.55 - 2.15	9.38 - 12.8		

Human*: C_{12h} and $AUC_{0\text{-}12\,h}$; 400 mg twice a day; HIV-1-infected patients
Human**: C_{24h} and $AUC_{0\text{-}24\,h}$; 300 or 600 mg once per day; HIV-1 infected patients
Human***: C_{24h} and $AUC_{0\text{-}24\,h}$;120 or 200 mg once per day; HIV-1 infected patients

FIG 5 Drug pharmacokinetic analysis in hu-NSG mice receiving oral three-drug cART. (A) At different time point postinitiation of cART, the drug concentrations (raltegravir, tenofovir, and emtricitabine) within the plasma of mice blood by LC-MS. (B) Mean value of drug concentration (C_{24} and C_{72}) and area under the curve (AUC) during 24 or 72 h (AUC_{0-24} and AUC_{0-72}). N, number of tested mice = 4 females and 4 males; AUC_{0-24} or AUC_{0-72}, area under the concentration-time curve from 0 to 24 or 0 to 72 h postdose (in μg·h/ml); C_{24} or C_{72}, concentration at 24 or 72 h postdose (in μg/ml). Data are presented as means ± the SD.

Drug pharmacokinetics analysis in hu-NSG mice receiving oral ART. We further determined the pharmacokinetic profile of each drug in plasma of hu-NSG mice receiving three-drug ART regimen. We calculated human-equivalent doses—a 400-μg total dose of raltegravir, a 2,140-μg total dose of tenofovir disoproxil fumarate, and a 100-μg total dose of emtricitabine—based on K_m values of 37 and 3 for humans and mice, respectively, as described previously (36). At different time point postinitiation of cART, we collected the peripheral bloods from individual mouse and analyzed the drug concentrations (raltegravir, tenofovir, and emtricitabine) within the plasma by liquid chromatography-mass spectrometry (LC-MS).

After oral administration of this three-drug ART regimen to each mouse weighing at around 30 g, the three drugs showed a dynamic distribution (from 24 to 72 h postdose) and elimination (from 72 to 168 h postdose) (Fig. 5A). A peak concentration at 72 h postdose was observed in the majority of animals receiving the three-drug ART regimen. The mean drug concentration (C_{24} and C_{72}) and area under the curve (AUC) for 24 or 72 h (AUC_{0-24} and AUC_{0-72}) that is regularly used as a generic outcome predictor of drugs activity were showed in Fig. 5B.

Clinical pharmacokinetic profile (PK) of raltegravir in HIV-1-infected patients showed that a dose of 400 mg twice daily of raltegravir achieved a C_{12} concentration ranging from 0.040 to 0.399 μg/ml and an AUC_{0-12} ranging from 9.5 to 13.4 μg·h/ml (37). In the present study, the total 400-μg dose of raltegravir in hu-NSG mice that resulted in the C_{24} was 0.143 to 0.168 μg/ml, and the AUC_{0-24} was 3.44 to 4.02 μg·h/ml in male and female animals. Although we could not find the clinical PK profile for humans at the same time point in the literature (37, 38), our data demonstrated that the overall raltegravir exposure with a 400-μg dose was within the range of variability seen in humans receiving 400 mg twice a day. Furthermore, oral administration of 2.14 mg of tenofovir disoproxil fumarate and 100 μg of emtricitabine resulted in a comparable drug C_{24} observed in HIV-1 patients (39–41).

Although C_{24} and AUC_{0-24} were similar in male and female animals given a total 400-μg dose of raltegravir, the female group showed a faster drug distribution/elimination during period from 24 to 168 h postdose. Specifically, raltegravir presented a 2.7-fold-higher exposure at 72 h in the female group than what was observed in male group (the AUC_{0-24} of the female group was 82.58 μg·h/ml versus 30.10 μg·h/ml for the male group, Fig. 5B), suggesting sex differences in the pharmacokinetics of raltegravir. Similarly, the experimental male and female groups also exhibited differences in their responses to tenofovir and emtricitabine. Relatively higher tenofovir and emtricitabine AUCs were observed in the female groups than in the male groups (ca. 1.5- to 3.0-fold higher) at both 24 and 72 h postdose. Collectively, our results demonstrated that hu-NSG mice receiving oral ART displayed similar pharmacokinetic profiles in humans and support sex-related differences in drug pharmacokinetics (42, 43). The hu-NGS model may be useful for understanding clinically important gender-related differences in HIV treatment.

Human resting CD4$^+$ T cells constitute a substantial cell population in the peripheral blood and lymphoid tissue of humanized NSG mice. Resting memory CD4$^+$ T cells, which are the best-characterized HIV reservoir, have been clinically detected in human blood, lymph node, and gut tissues (3, 5, 44). To confirm the relevance of the hu-NSG model, we determined the presence of human resting CD4$^+$ T cells in hu-NSG mice at 12 to 14 weeks posttransplantation. We used flow cytometry analysis of mononuclear cells isolated from various tissues (peripheral blood, intestine, spleen, liver, and bone marrow) to show the levels of human CD4$^+$ T cells ranging from 17.5 to 64.4% of all T cells (Fig. 6A). Of these, 27 to 71.9% were of the CD45RO$^+$ CD27$^+$ subpopulation, suggesting the presence of the central memory CD4$^+$ T cell lineage (Fig. 6B). We used negative selection to isolate resting human CD4$^+$ T cells from peripheral blood and spleen for multicolor flow cytometry analysis. The recovered cells population are CD25 negative (an early activation marker). Within the CD4$^+$ T cell population in both peripheral blood and spleen, we observed a homogeneous population of human CD4$^+$ CD45RO$^+$ CD45RA$^-$ CCR7$^+$ CD27$^+$ CD25$^-$ CD62L$^+$ CD2$^+$ CD7$^+$ resting T cells (Fig. 6C and D). Specifically, in the human CD4$^+$ T cell population, as shown with 25.7 or 25% of the CD3$^+$ CD4$^+$ population, we found a higher level (99.6 or 90%) of the human CD45RO$^+$ CD45RA$^-$ subpopulation, which further demonstrated a varying level of CD27$^+$ CCR7$^+$ subpopulation, as gated with 25.7 and 56% in both the peripheral blood and spleen, respectively. In addition, $>$40% cells were CD25 negative but CD62L positive in the human CD45RO$^+$ CD45RA$^-$ subpopulation, confirming that they were from the resting memory cell lineage. Taken together, we demonstrated that peripheral blood and lymphoid organs are the sources of human resting memory CD4$^+$ T cells in the hu-NSG mice.

Human resting CD4$^+$ T cells from hu-NSG mice on suppressive cART contain replication-competent HIV. Although prolonged cART therapy suppresses HIV replication below the detectable level, HIV persists as a transcriptionally inactive provirus in resting memory CD4$^+$ T cells; this so-called latent reservoir has a long half-life and prevents HIV eradication by cART alone (8). HIV latency may be reversed by inducing resting CD4$^+$ T cell activation and subsequent release of infectious viruses capable of new infection (45, 46). To determine whether a latent HIV reservoir exists in the resting CD4$^+$ T cells isolated from cART-treated aviremic hu-NSG mice, we conducted a viral outgrowth assay (VOA). This assay is the current standard for determining the size of the latent HIV reservoir (47, 48) and measures the frequency of resting CD4$^+$ T cells that produce infectious virus after a single round of maximum *in vitro* T cell activation.

As described above (Fig. 3A), we treated HIV-infected hu-NSG mice with cART for 6 weeks, resulting in no detectable plasma viremia in all experimental animals. We collected mononuclear cells from peripheral blood, gastrointestinal tract, spleen, bone marrow, and liver and pooled these cells for human resting memory CD4$^+$ T isolation by negative selection as described above. Subsequently, we maximally activated the isolated resting CD4$^+$ T cells using the mitogen phytohemagglutinin (PHA), which is regularly used to reverse latency in the standard VOA protocol. We expanded released

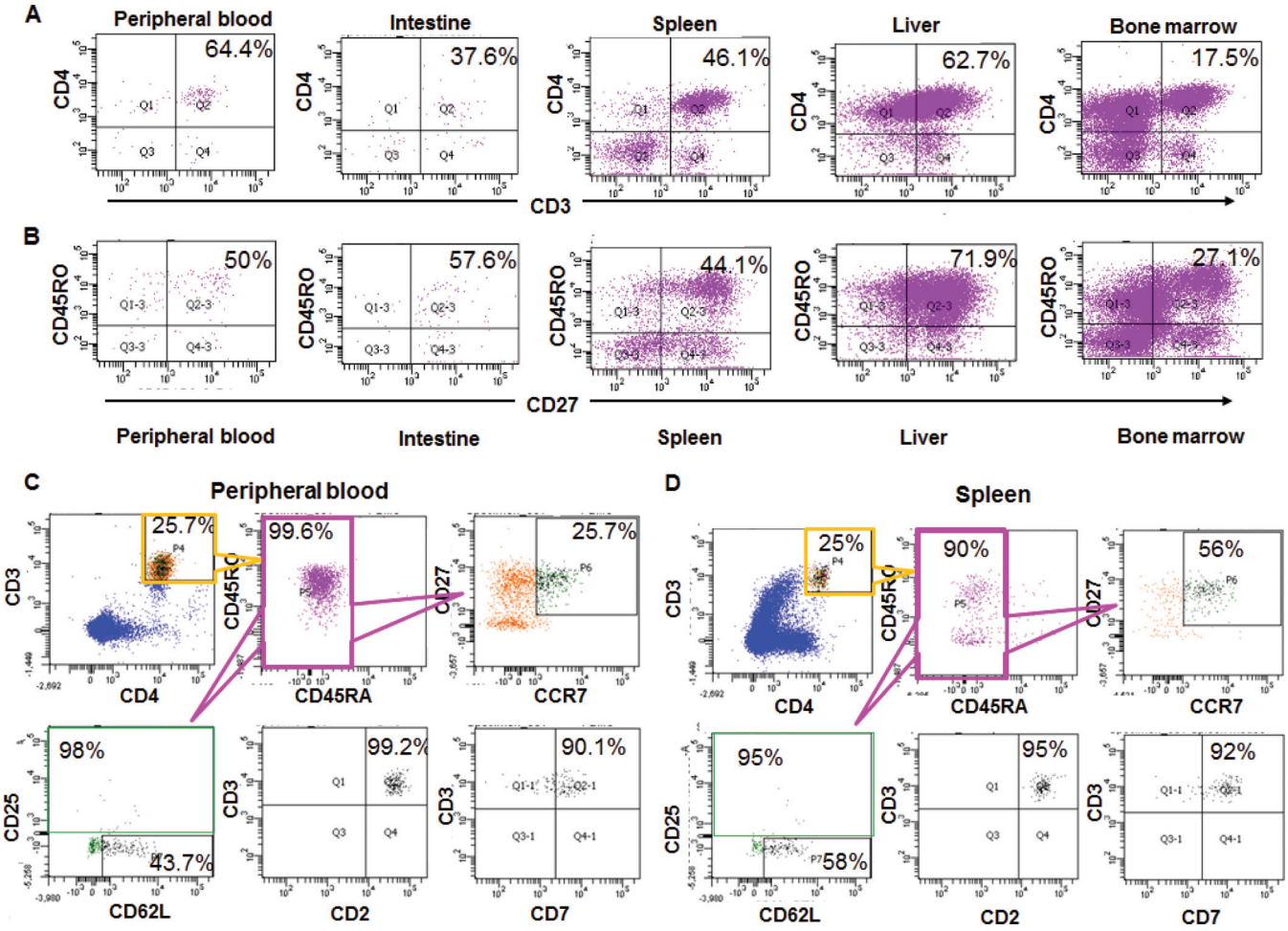

FIG 6 Presence of human resting memory CD4$^+$ T cells in hu-NSG mice. (A) Flow cytometry analysis of CD4$^+$ T mononuclear cells from various tissues in hu-NSG mice, including peripheral blood, intestine, spleen, liver, and bone marrow. (B) Flow cytometry analysis of CD45RO$^+$ CD27$^+$ subpopulation (central memory T cells) within the CD4$^+$ T cells from various tissues as described above. (C and D) After negative selection, flow cytometry analysis of mononuclear cells from peripheral blood (C) and spleens (D) was performed with human antibodies for CD4, CD3, CD45RA, CD45RO, CCR7, CD27, CD62L, CD25, CD2, and CD7 (resting T cells). The flow analysis results for a representative mouse are shown.

viruses by coculture with CD8-depleted, activated PBMCs from HIV-negative donors. We measured viral growth in culture supernatants using enzyme-linked immunosorbent assay (ELISA) for HIV p24 antigen level and determined the frequency of resting cell infection using a maximum-likelihood method as described by Siliciano et al. (48). Due to the limited number of cells isolated from hu-NSG mice, we were only able to calculate the frequency of resting cell infection (RCI) for two of three individual mice, which showed a range of 2 to 3 infectious units per million (IUPM) resting CD4$^+$ T cells (Fig. 7). These results demonstrated that HIV infection in hu-NSG mice results in the establishment of a population of resting CD4$^+$ T cells that can be isolated and induced to produce replication-competent HIV *ex vivo*.

DISCUSSION

Immunodeficient mice that are repopulated with human cells and/or implanted with human tissues (i.e., "humanized mice") have been developed to investigate HIV replication, transmission, immune response, and pathogenesis and to evaluate various HIV eradication strategies (10). For instance, humanized bone marrow/liver/thymus (BLT) mice (23, 27) and severe combined immunodeficiency-human-thymus/liver mice (SCID-hu-thy/liv) (18) that are repopulated with human immune cells and/or implanted human tissues have been developed for screening antiviral agents, identifying latently

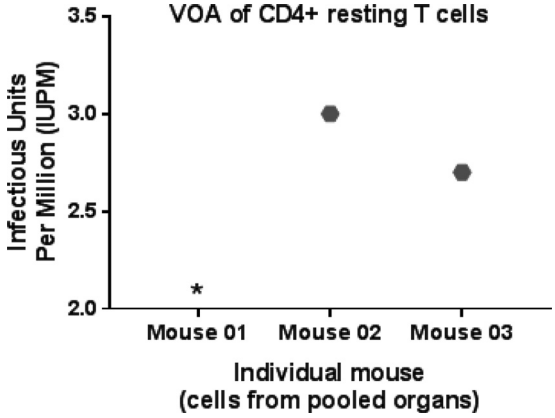

FIG 7 Determination of IUPM in resting CD4$^+$ T cells by VOA. Resting human CD4$^+$ T cells were isolated from an individual HIV-infected hu-NSG mouse with nondetectable viral loads at harvest. The frequency of latently infected cells in each animal was determined according to a standard clinical protocol. The asterisk (*) indicates an inability to collect enough cells from mouse 01 for the test. The confidence intervals for individual determinations were ±0.7 log IUPM.

infected T cells, and establishing treatment approaches for HIV research. However, these models require laborious surgical manipulation and time-consuming human cell reconstitution. In the hu-NSG model, human T cell maturation occurs in mouse thymic environment, and T cell selection takes place in the context of mouse major histocompatibility complex proteins, limiting human leukocyte antigen (HLA)-restricted function (13, 49). Despite the limitation, the human HSC-engrafted NSG model (hu-NSG) model at least partially supported the maturation of human T and B cells, as evidenced by the development of human B cells, as well as human CD4$^+$ and CD8$^+$ T cells in secondary lymphoid organs. Although the hu-NSG model, which clearly recapitulates key aspects of HIV infection and pathogenesis, represents a more flexible and surgery-free alternative for the study of HIV in humanized mice (50), there is currently no systemic analysis of HIV replication, therapy response, HIV latency, and persistence in the hu-NSG model on suppressive cART. For this reason, in this study, we validated the use of hu-NSG mouse model for studying HIV infection, therapy response, and HIV latency. We confirmed that the HIV-infected hu-NSG mouse model recapitulates key aspects of HIV infection and pathogenesis *in vivo*. In addition, we demonstrated the ability HIV-infected human cells isolated from HIV-infected hu-NSG mice on suppressive cART to act as a latent HIV reservoir.

Our results verified that human hematopoietic cells are present in all the examined tissues of hu-NSG mice, including peripheral blood and primary/secondary lymphoid tissues. Consistent with previous reports (22), we demonstrated that the hu-NSG mouse model supports HIV replication and CD4$^+$ T cell depletion after infection with HIV CCR5-tropic virus. In addition, we observed that the CD4$^+$ T cells and CD68$^+$ macrophages were diffusely distributed in the cervical-vaginal area, suggesting that this model may support HIV infection via vaginal exposure. In a recent study (Shasha Li and John Burnett, unpublished data), we evaluated hu-NSG mice for their susceptibility to HIV-1 infection via the vaginal route. These data demonstrated that CCR5-tropic HIV-1 BaL virus infection by the vaginal route led to productive infection and sustained viremia in female hu-NSG mice.

Although both the hu-NSG and BLT models respond robustly to HIV-1 infection (10), different susceptibilities to HIV-1 were observed between these two models. A lower viremia level was observed in our hu-NSG model after 2 weeks post-HIV-1 CCR5-tropic BaL virus infection, indicating plasma viral loads averaging 10^4 per ml versus 10^6 per ml in BLT mice challenged with either CCR5-tropic JR-CSF or CXCR4-tropic NL4-3 virus (23, 27, 51, 52). Since different HIV-1 viruses (with various HIV p24, ca. 50 to 250 ng) and infection procedures (e.g., i.p. injection, intravenous injection through the retro-orbital

or tail vein, or mucosal infection intravaginally) were used in these studies, variation in the viral loads between the two models is somewhat expected. However, our results, along with others, demonstrated the capacity of the hu-NSG model to support consistent infection and sustained viremia (22).

Our results show that oral administration of a preformulated three-drug cART cocktail (TDF, FTC, and RAL) efficiently interrupts the exponential growth of the virus and reduces plasma viral RNA to undetectable levels within 4 weeks posttreatment. After the initial control of viremia, all animals treated with three-drug cART exhibited undetectable plasma viral loads for the full 6-week course of suppressive therapy with no detectable viral blips, indicating the potency and consistency of this ART regimen. In several previous studies, the three-drug cART regimen was administered via the parenteral route (i.p. injections or subcutaneous injections) to an HIV-infected BLT mouse model (27) and a macaque SIV model (53) to rapidly suppress viremia. Similarly, Choudhary et al. demonstrated that plasma viral loads were suppressed below limit of detection in hu-Rag2$^{-/-}$ γc$^{-/-}$ mice administered a four-drug ART regimen via the parenteral route (54). However, the administration of cART drugs via the parenteral route is quite cumbersome and time-consuming and, due to biosafety concerns, is not a very attractive option in HIV-infected mice. Supplementation in the drinking water or feed is a more convenient and less stressful way to administer commonly used drugs. Several recent studies demonstrated that oral administration of antiretroviral drugs could potently reduce HIV-1 plasma viral loads and provide preexposure prophylaxis for the transmission of HIV-1. For example, 4′-ethynyl-2-fluoro-2′-deoxyadenosine (EFdA), a nucleoside analog reverse transcriptase inhibitor that was reconstituted in phosphate-buffered saline (PBS) and administered orally to BLT mice by oral gavage, efficiently inhibited HIV-1 replication in gastrointestinal and female reproductive tracts of humanized BLT mice (55). Similarly, a single-drug or a two-drug regimen (RAL, EFdA, or TDF plus FTC) were freshly dissolved in various buffers and then administered by oral gavage to a BALB/c-Rag2$^{-/-}$ γc$^{-/-}$ (RAG-hu) mouse model (56), a SCID-hu Thy/Liv and BLT mouse model, and a rhesus macaque model (57), consequently providing a rapid suppression of HIV-1 viremia. However, compounding a medication into a secondary matrix, such as a drinking water formulation, might alter the stability, purity, or even potency of the active ingredients. In this study, we utilized a sweetened water gel suspension, MediDrop sucralose (ClearH_2O, Westbrook, ME) to deliver the antiretroviral drugs. MediDrop sucralose is an oral formulation that is advertised to aid with water bottle medication delivery. Our results demonstrate that the oral three-drug cART regimen can reliably suppress viremia as efficiently as the parenteral four-drug ART regimen previously reported (27, 54). The drinking water formulation suppressed viremia to below the level of detection, which not only prevented further decline in CD4$^+$ T cells but also resulted in an increased CD4$^+$ T cell percentage in the peripheral blood of all the tested mice.

Furthermore, drug pharmacokinetic (PK) analysis demonstrated that hu-NSG mice receiving oral ART have a PK profile similar to that observed in human patients. Female and male animals responded differently to drug treatment. Since it is clinically critical to rationally design safe and effective antiretroviral regimens for individuals, our hu-NSG model would be a useful tool for conducting risk assessment and understanding sex-related differences in drug pharmacokinetics in HIV treatment.

During the treatment interruption, patients taking cART often show a rapid rebound of plasma viremia to levels comparable to those detected prior to the initiation of therapy (58). In our study, discontinuation of cART therapy after viral suppression resulted in rapid viral rebound and loss of peripheral CD4$^+$ T cells, demonstrating that this model recapitulates key aspects of human HIV infection. These observations, which were consistent with viral dynamics seen in HIV human studies, suggest that hu-NSG mice are permissive to HIV infection and primed for a dynamic response to oral cART and/or disruption of treatment, thus providing a reliable and facile animal model for studying HIV infection.

Furthermore, cART affected systemic virus production; cART dramatically reduced

vRNA and vDNA levels in lymphoid tissues compared to the untreated control group. However, the least pronounced reduction in vRNA and vDNA levels were noted in the brain, suggesting that cART penetration is limited in the CNS and may limit the ability of cART to suppress HIV replication (Fig. 4C) (35). The blood-brain barrier restricts the movement of immune cells and chemotherapeutic drugs, and therefore the CNS could potentially act as a sanctuary compartment where the viral particles can survive in an immune-privileged environment (59).

Despite the fact that cART can achieve levels of HIV-1 RNA in plasma (viral load) that are practically undetectable, there is emerging evidence for residual viral replication in patients on suppressive cART (1). HIV persistence during cART can be due to latently resting $CD4^+$ T cells in either preintegration or postintegration phases of infection. The largest latent HIV reservoir is resting memory $CD4^+$ T cells (60). We therefore sought to demonstrate the presence of resting $CD4^+$ T cells in the naive hu-NSG mice. Our results show that memory $CD4^+$ T cells constitute the major cell population in several lymphoid tissues, including the intestine, spleen, and bone marrow, in addition to peripheral blood. Choudhary et al. observed that 48 to 50% of cells were $CD45RO^+$ memory $CD4^+$ T cells in naive hu-Rag2$^{-/-}$ $\gamma c^{-/-}$ mice (54). These researchers reported that the majority of memory $CD4^+$ T cells lacked activation markers such as CD25, CD69, and HLA-DR, suggesting that the lymphoid tissues in this humanized mouse would provide the milieu necessary for the maintenance of resting memory $CD4^+$ T cells. Similarly, resting $CD4^+$ T cells have been demonstrated in the peripheral blood and primary/secondary lymphoid tissues of naive BLT mice, as demonstrated by the expression of CD4, CCR7, and CD27 and lack of expression of CD8, CD25, HLA-DR, and CD11b (27). The marked expression of CD45RO, CCR7, CD27, CD62L, CD2, and CD7 on the resting $CD4^+$ T cell populations in our study suggests that these resting cells can support infection within lymphoid tissue similar to that observed in HIV-infected patients. In addition, our VOA results demonstrated that the resting $CD4^+$ T cells isolated from cART-treated aviremic hu-NSG mice harbor replication-competent virus, thus supporting the presence of a latent reservoir in this model. Future analysis of sorted cell subpopulations, primarily central memory and transitional memory $CD4^+$ T lymphocytes, to investigate the presence of proviral DNA would be warranted in our hu-NSG model. Taken together, we demonstrated that the resting $CD4^+$ T cells of the hu-NSG mice on suppressive cART constitute a latent HIV reservoir.

In conclusion, our data establish that cART consisting of a well-characterized combination of three FDA-approved therapeutic antiretroviral drugs administered as an oral drinking formulation is capable of suppressing HIV replication in hu-NSG mice, and we demonstrate that, as in humans and nonhuman primates, the infection persists for the duration of the treatment. We have also shown the extensive presence of memory $CD4^+$ T cells harboring replication-competent HIV, a major reservoir of known importance for the eradication of HIV-1 infection in humans. Collectively, given the relatively short time frame time necessary to observe suppressive cART efficacy in this model, our study improves our knowledge of the systemic effects of cART *in vivo* and demonstrates that the hu-NSG mouse model is a valuable *in vivo* tool for preclinical evaluation of antiretroviral therapy, HIV replication, latency and persistence, and eradication strategies.

MATERIALS AND METHODS

Materials. Unless otherwise noted, all chemicals were purchased from Sigma-Aldrich, all restriction enzymes were obtained from New England BioLabs (NEB) and all cell culture products were purchased from GIBCO (Gibco BRL/Life Technologies, a division of Invitrogen). Other reagents included Moloney murine leukemia virus reverse transcriptase and random primers (Invitrogen), reverse transcriptase iScript (Bio-Rad), HIV-1 BaL NIH AIDS Research and Reference Reagent Program, a human $CD34^+$ enrichment by magnetic-activated cell sorting (MACS) system (Miltenyi Biotec), a human resting $CD4^+$ T cell enrichment with a mouse/human enrichment kit (EasySep Human Memory $CD4^+$ T cell enrichment kit; Stemcell Technologies), and a DNeasy blood and tissue kit (Qiagen).

Ethics statement. All animal care and procedures have been performed according to protocols reviewed and approved by the City of Hope Institutional Animal Care and Use Committee (IACUC) held by the principal investigator for this application (John Rossi, IACUC 12034). Human fetal liver tissue was

obtained from Advance Bioscience Resources (Alameda, CA), a nonprofit organization, in accordance with federal and state regulations. The vendor has its own Institutional Review Board (IRB) and is compliant with human subject protection requirements.

The research involves blood specimens from anonymous human subjects with no identifiers for age, race, ethnicity, or gender. All human tissue specimens is obtained from healthy, anonymous donors from third party sources. We use discarded peripheral blood from anonymous, healthy adult donors from the City of Hope Blood Donor Center (Duarte, CA), for isolation of PBMCs and subsequent primary $CD4^+$ T cell cultures. The information provided for the above was evaluated and determined to not involve human subjects research [45 CFR 46.102(d)(f)]. Therefore, it does not need to be approved, nor does it need to undergo continuing review by the IRB in the City of Hope (IRB reference no. 97071/075546).

Generation and characterization of humanized NOD/SCID/IL2rγ^{null} mice (hu-NSG). (i) Isolation of hematopoietic stem/progenitor cells. Human $CD34^+$ HSCs were isolated from fetal liver tissue obtained from Advance Bioscience Resources according to regulatory guidelines. The fetal liver tissue (16 to 24 weeks of gestation) was treated with collagenase digestion, followed by filtration through sterile 70-μm-pore size nylon mesh filter. Immunomagnetic enrichment for $CD34^+$ cells was performed using a MACS system, according to the manufacturer's instructions, with the modification that the initial purified $CD34^+$ population was put through a second column and washed three times with 3 ml of the supplied buffer per wash before the final elution. This additional step gave a >99% pure $CD34^+$ population, as measured by flow cytometry analysis using anti-CD34 antibody.

(ii) Injection of human $CD34^+$ HSCs in NSG mice. NOD.Cg-Prkdc scid Il2rg tm1Wj/SzJ (NOD/SCID/IL2rγ^{null} [NSG]) mice were obtained from Jackson Laboratories. A modified intrahepatic injection technique was used for engraftment of neonatal pups within 48 h of birth. A custom-made Hamilton 80508 syringe/needle set-up was used for the injections. The needle specifications are 30 gauge, 51-mm-long needle with a beveled edge attached to a 50-μl glass syringe. The maximum volume used for injection with this needle/syringe was 25 μl. Animals were preirradiated with 100 cGy and then transplanted with 0.5×10^6 to 1×10^6 $CD34^+/CD90^+$ HSCs each. At 12 to 14 weeks after transplantation, blood was collected, and the engraftment was verified using multiparameter flow cytometry analysis.

(iii) Mouse blood and tissue collection. Peripheral blood samples were collected at approximately 10 to 12 weeks of age using retro-orbital sampling. Red blood cells were lysed using Red Cell lysis buffer solution (Sigma-Aldrich), and the remaining cells were washed with PBS. This was followed by blocking in fetal bovine serum (FBS) and further staining for flow cytometry analyses. Tissue samples were collected at necropsy and processed immediately for cell isolation and flow cytometry analysis. Tissue samples were manually agitated in PBS before filtering through a sterile 70-μm-pore size nylon mesh screen (Fisher Scientific), and suspension cell preparations were produced as previously described (22, 24). Intestinal samples were processed according to a published protocol (22), with the modification that the mononuclear cell population was isolated after incubation in citrate buffer and collagenase enzyme for 2 h, followed by nylon mesh filtration and Ficoll-Hypaque gradient isolation (GE Healthcare).

(iv) Flow cytometric analysis of human leukocytes in peripheral blood (PB) and tissue. Flow cytometry analysis of human cells was performed using a FACSCalibur instrument (BD Biosciences), BD Fortessa (BD Biosciences), and FlowJo software version 8.8.6. The gating strategy performed was an initial forward-scatter versus side-scatter (FSC/SSC) gate to exclude debris, followed by a human CD45 gate. For analysis of lymphocyte populations in peripheral blood, a further lymphoid gate (low side scatter) was also applied to exclude cells of monocytic origin. All antibodies used were fluorochrome conjugated, human specific, and obtained from BD Biosciences: phycoerythrin (PE)/Texas Red-conjugated anti-CD45 (clone 2D1), PE-conjugated anti-CD19 (clone HIB19), allophycocyanin/Alexa Fluor 750-conjugated anti-CD14 (clone MϕP9), peridinin-chlorophyll protein/Cy7-conjugated anti-CD3 (clone SK7), pacific blue-conjugated anti-CD4 (clone SK3), fluorescein isothiocyanate-conjugated anti-CD8 (clone HIT8a), and brilliant violet-conjugated anti-CCR5 (2D7). Gates were set using fluorescence minus one controls, in which cells were stained with all antibodies except the one of interest. Specificity was also confirmed using isotype-matched nonspecific antibodies (BD Biosciences) and with tissues from animals that had not been engrafted with human cells (data not shown).

Histopathology. Samples of skin, lung, liver, spleen, small/large intestine, reproductive tract, and brain tissue from hu-NSG mice were examined 13 to 14 weeks posttransplantation. These samples were fixed with 10% formaldehyde, embedded in paraffin, and stained with hematoxylin and eosin (H&E). Tissues were also collected and placed in fresh phosphate-buffered 4% paraformaldehyde (PFA) for 4 to 6 h, washed with 80% ethanol, and stored in 80% ethanol until being embedded in paraffin. Immunohistochemical staining was performed on 5-μm-thick sections from PFA-fixed, paraffin-embedded tissue. Tissue sections were placed on slides and deparaffinized in xylene, followed by grades of ethanol. Slides were quenched in 3% hydrogen peroxide, heat-induced epitope retrieval was performed, and slides were incubated in blocking buffer. Slides were washed, incubated for 30 min with primary antibody in dilution buffer, washed, incubated in secondary antigen (avidin/biotin tag), washed again, and incubated with the chromogen diaminobenzidine tetrahydrochloride (DAB). Slides were rinsed in distilled H_2O, counterstained with hematoxylin, rinsed in distilled H_2O, rehydrated through grades of alcohol and xylene, and mounted. The following primary antibodies used for immunohistochemistry were human specific and obtained from Dako: anti-CD4, anti-CD8, anti-CD20, anti-CD68, anti-CD14, anti-CD45, and anti-CD3. DAB staining was performed using a Ventana Ultraview DAB detection kit in a Ventana BenchMark XT processor (Ventana Medical Systems, a division of Roche). Sections stained with isotype-matched control antibodies did not show staining in these tissues (data not shown). In addition, staining of a nonhumanized mouse with the same primary and secondary antibodies was also used as an additional control (data not shown).

***In vivo* HIV-1 challenge with hu-NSG mice.** A cell-free virus stock of CCR5-tropic HIV-1 clone BaL was obtained from the AIDS Research and Reference Reagent Program, Division of AIDS, NIAID, NIH. HIV BaL virus was propagated in human PBMCs and harvested at 10 days postinfection. Virus was titrated using the Alliance HIV-1 p24 ELISA kit (Perkin-Elmer).

Hu-NSG mice with stable human leukocyte reconstitution (with a 20% or higher percentage of human CD45$^+$ T cells) were infected i.p. with HIV BaL (200 ng of p24/mouse) while under inhalant general anesthesia. Plasma viremia was assayed using one-step reverse transcriptase real-time PCR (TaqMan assay) with an automated CFX96 Touch Real-Time PCR detection system (Bio-Rad). HIV-1 level in peripheral blood was determined by extracting RNA from 5×10^5 cells using the QIAamp Viral RNA minikit (Qiagen) and performing TaqMan qPCR with a primer and probe set targeting the HIV-1 LTR region, using a TaqMan Fast Virus 1-Step master mix (Thermo Fisher). According to the manufacturer's instructions (QIAamp Viral RNA minikit [Qiagen]), the protocol is designed for purification of viral RNA from a minimal 140 μl of plasma. In a standard TaqMan qPCR-based HIV-1 plasma viral load test, the limit of detection (LOD) is typically about 40 RNA copies/ml when viral RNA isolated from 140 μl of plasma sample is applied. In our animal study, the plasma sample was expanded by dilution (generally one to three dilutions) because only limited volume of plasma (ca. 50 to 80 μl) was available from preterminal bleeds. The LODs of the diluted samples were around 110 to 160 RNA copies/ml under these experimental conditions. Therefore, we defined values below that LOD as undetectable.

Oral administration of cART in HIV-infected hu-NSG mice. Infected mice with demonstrable viral infection were treated for 6 weeks with cART composed of drugs that block new infections, without inhibiting viral production in infected cells. The cART regimen consisting of tenofovir disoproxil fumarate (TDF; 300 mg/capsule), emtricitabine (FTC; 200 mg/capsule), and raltegravir (RAL; 400 mg/capsule) (Novartis and Gilead Sciences), scaled down to the equivalent mouse dosage using the appropriate conversion factor, was administered in a drinking water formulation (sweetened water gel; Medidrop Sucralose). We calculated human-equivalent doses of ~0.4 mg (total dose) of RAL, ~0.1 mg (total dose) of FTC, and ~2.14 mg (total dose) of TDF based on K_m values of 37 and 3 for humans and mice, respectively (36). The medication tablets were powdered thoroughly and resuspended in the sweetened water gel formulation. Mice were bled by retro-orbital route, and plasma viral loads and CD4$^+$ T cell populations were assayed every 2 weeks. Mice that had suppressed or undetectable plasma viral loads were monitored for 6 weeks, at which time, the cART regimen was withdrawn. The mice were bled and assayed for rebound of plasma viremia and CD4$^+$ T cell population every 2 weeks until sacrifice.

Quantitative LC-MS/MS analysis of tenofovir, emtricitabine, and raltegravir in HIV-infected hu-NSG mice. (i) Description and definition of LC-MS/MS parameters. Liquid chromatography-tandem mass spectrometry (LC-MS/MS) instrumentation consisted of a Shimadzu Prominence high-pressure liquid chromatography (HPLC) system (Columbia, MD) interfaced to an AB SCIEX QTRAP 5500 system (Foster City, CA). HPLC separation was achieved using a Waters Atlantis T3 analytical column (3 μm, 150 by 2.1 mm; Milford, MA) preceded by a Phenomenex C_{18} guard column (Torrance, CA). The column temperature was maintained at 40°C, and the flow rate was 0.3 ml/min. The mobile phases consisted of 0.1% formic acid in deionized water (mobile phase A) and 0.1% formic acid in acetonitrile (mobile phase B). The following gradient program was used: 5% B to 95% B (0 to 5 min) and 5% B (5 to 6 min). Under optimized assay conditions, the retention times for tenofovir/tenofovir-d6, emtricitabine, and raltegravir were 1.44, 1.63, and 4.83 min, respectively, and the total run time was 6 min. The electrospray ionization source of the mass spectrometer was operated in positive-ion mode, and the detector settings were optimized to result in abundant protonated molecular ions (MH^+) of 288.1, 294.1, 248.0, and 445.2 for tenofovir, tenofovir-d6, emtricitabine, and raltegravir, respectively. The following precursor with or wihtout product ion combinations were used in multiple-reaction monitoring mode for quantitation: 288.1 $\pm$ 176.1 *m/z* (tenofovir), 294.1 $\pm$ 182.4 *m/z* (tenofovir-d6), 248.0 $\pm$ 130.2 *m/z* (emtricitabine), and 445.2 $\pm$ 109.2 *m/z* (raltegravir). Analyst software version 1.5.1 was used for data acquisition and processing.

(ii) Drug quantification in mouse plasma. To prepare plasma samples for injection, 10 μl of an internal standard solution (10 μg/ml tenofovir-d6 in 50:50 acetonitrile-water) and 50 μl of methanol was added to 50 μl of plasma. After vigorous vortex mixing for 1 min, 100 μl of acetonitrile was added. The mixture was again vortex mixed for 1 min and then centrifuged at 10,000 $\times$ *g* for 5 min. The supernatant was transferred to a glass autosampler vial, and a final volume of 3 μl was injected on column. The AUC calculation was performed by multiplying the average by the sampling time (either 24 or 72 h).

(iii) Drug quantification in mouse plasma in mouse brain. For preparation of brain tissue samples, 150 μl of ice cold water and 10 μl of internal standard (10 μg/ml tenofovir-d6 in 50:50 acetonitrile-water) was added to 50 mg of brain tissue. Homogenization was performed using a Next Advance Bullet Blender (Averill Park, NY), and 50 μl of the resulting tissue homogenate was added to 50 μl of ice cold methanol. After vigorous vortex mixing for 1 min, 100 μl of acetonitrile was added. The mixture was again vortex mixed for 1 min and then centrifuged at 10,000 $\times$ *g* for 5 min. The supernatant was transferred to a glass autosampler vial, and a final volume of 10 μl was injected into the column.

Isolation of the resting CD4$^+$ T cell population from hu-NSG mice. Human mononuclear cells from the spleen, intestine/mesenteric lymph node, bone marrow, peripheral blood, and liver were enriched on 40 to 70% Percoll gradients by centrifugation (Percoll Plus; GE Healthcare, Piscataway, NJ). Cells were pooled from all tissues and resuspended at 5×10^7 cells/ml in recommended medium (Ca^{2+}- and Mg^{2+}-free PBS containing 2% FBS and 1 mM EDTA), and human resting CD4$^+$ T cells were enriched using a mouse/human enrichment kit (EasySep human memory CD4$^+$ T cell enrichment kit; Stemcell Technologies, catalog no. 19157) and negative magnetic selection with modifications. Briefly, the cells

were incubated with a cocktail of antibodies composed of anti-mouse CD45, CD31, CD105, and TER119 and anti-human CD8, CD14, CD16, CD19, CD56, CD41, CD25, CD31, CD36, CD56, CD61, CD66b, CD69, CD105, CD123, HLA-DR, gdTCR, biotin, and glycophorin A. The mouse and human antibodies were conjugated with anti-biotin tetrameric antibody complex and added at 50 and 65 μl/ml of cells, followed by incubation with magnetic colloids for 5 min. Antibody-bound cells were removed using a column based-magnetic purification system, and the purified resting cells were collected as flowthrough. This approach resulted in a >99% pure resting CD4$^+$ T cell population. The recovered cells population are CD25 negative (an early activation marker).

VOA. Viral outgrowth assay (VOA) was performed to quantify resting CD4$^+$ T cell infection. Cells isolated as described above were cultured for 2 days *in vitro* in 1 μM RAL and 15 nM efavirenz (Mylan Pharmaceuticals, Inc.) to block new viral infections. A p24 assay was performed using culture supernatant to confirm the absence of ongoing active viral replication in the cell population. The cells were washed and then replated at 1×10^4 or 1×10^5 cells/well in 12-well culture plates, followed by maximal activation for 2 days with 1 μg/ml PHA, 100 U/ml IL-2, and a 10-fold excess of irradiated, CD8-depleted PBMCs from an HIV-negative donor. PBMCs were added to the culture to allow for detection of low levels of viral replication. Control cultures received only 20 U/ml of IL-2 to maintain homeostatic conditions. The culture supernatant was removed every 3 to 4 days to maintain optimum pH and replaced with an equivalent volume of complete medium containing 20 U/ml IL-2. The HIV p24 level was measured to determine the extent of induction of viral replication at days 15 and 19 postisolation, and the cultures were scored as positive if p24 was detectable at 15 days after stimulation and confirmed on day 19. The infected cell frequencies were determined by a maximum-likelihood method and are expressed as infectious units per million (IUPM) resting CD4$^+$ T cells as described by Siliciano et al. (48). In brief, as described previously, we obtained few millions of purified resting CD4$^+$ T cells from HIV-1-infected hu-NSG mice on suppressive cART. The VOA assay was set up as 5-fold dilution series (ranging from a million to less than a thousand cells per well), where the initial cell number depended on the total cell number isolated from the animals. Since one of three experimental mice did not have enough resting memory CD4$^+$ cells (less than a million) for dilution series as described, we could not represent the result as the IU per million cells (although there was p24 reading that we got). Accordingly, the cell-free supernatant was collected for HIV-1 p24 antigen test as described. The positive p24 readings were recorded in each tested well. Therefore, frequencies were determined from a tabulated set of calculated frequencies representing the maximum-likelihood estimate for each possible outcome in such a dilution series. Specifically, purified resting CD4$^+$ T cells isolated from two hu-NSG animals were cultured in duplicate or triplicate 5-fold dilution series as follows: 1,000,000, 200,000, 40,000, 8,000, 1,600, and 320 cells per well or 800,000, 160,000, 32,000, 6,400, 1,280, and 256 cells per well. One of two wells that contained 200,000 cells and one of three wells that contained 160,000 cells showed a positive p24 readout, providing a maximum-likelihood estimate for infection frequency as IUPM of 3.0 and 2.7, respectively. The confidence intervals for individual determinations were $\pm$0.7 log IUPM. The stable can be obtained from the ACTG Virology Core (48). In addition, several web-based tools are also available for IUPM assays (http://silicianolab.johnshopkins.edu/).

Quantitative RT-PCR analysis of HIV infection in HIV-infected hu-NSG mice. (i) DNA and RNA isolation from tissues or peripheral blood. Total DNA was isolated by using a DNeasy blood and tissue kit (Qiagen). The copy number of HIV-1 was normalized to 10^6 copies of GAPDH (glyceraldehyde-3-phosphate dehydrogenase) standard. Similarly, total RNA was isolated using the RNeasy minikit (Qiagen). The resultant cDNA was used for further qRT-PCR analysis.

(ii) Quantitative RT-PCR analysis. qRT-PCR experiments were performed using an iCycler iQ5 Real-Time PCR detection system (Bio-Rad). Total RNA was reverse transcribed using iScript cDNA synthesis kit (Bio-Rad) with 1 μg of total RNA. Amplification was performed with an amount of cDNA equivalent to 100 ng of total RNA. Calculations were performed using Bio-Rad software and the comparative threshold cycle (C_T) method and expressed as $2-\exp(\Delta\Delta C_T)$ using peptidylprolyl isomerase A (PPIA) as an internal control. The copy number of HIV-1 was normalized to 10^6 copies of the GAPDH standard.

Statistical analysis. Unless otherwise noted, error bars in all figures represent standard deviations (SD) or standard errors of the mean (SEM). GraphPad Prism software was used for statistical analyses, and differences were considered statistically significant when $P < 0.05$.

SUPPLEMENTAL MATERIAL

Supplemental material for this article may be found at https://doi.org/10.1128/JVI.02118-17.

SUPPLEMENTAL FILE 1, PDF file, 0.3 MB.

ACKNOWLEDGMENTS

This study was supported by the National Institutes of Health (grants R01AI29329 to J.J.R. and R01AI42552 and R01HL07470 to J.J.R. and J.C.B.) and the National Cancer Institute of the National Institutes of Health (grant P30CA033572 to support City of Hope Integrative Genomics, Analytical Pharmacology, and Analytical Cytometry Cores). Funding for the open-access charge was provided by the National Institutes of Health.

The content is solely the responsibility of the authors and does not necessarily represent the official views of the National Institutes of Health.

The reagent HIV BaL virus was obtained through the NIH AIDS Research and Reference Reagent Program, Division of AIDS, NIAID, NIH. We thank the City of Hope Animal Resources Center (ARC) for their support with animal use and care, the Analytical Cytometry Core for cell sorting and technical assistance with flow cytometry analysis, the Pathology Core for postmortem analysis of blood and tissue specimens, and the Analytical Pharmacology Core for pharmacokinetic analysis of antiretroviral drugs *in vivo*. Finally, we thank Sarah T. Wilkinson (scientific writer of City of Hope) for helpful advice in scientific writing. We also thank David DiGiusto of Stanford University, Paula Cannon of the University of Southern California, and Jerry Zack and Scott Kitchen of the University of California, Los Angeles, for assistance with technical aspects of various humanized HIV mouse models.

J.J.R. and J.Z. have an issued patent entitled "Cell-type-specific aptamer-siRNA delivery system for HIV-1 therapy" (USPTO, US 8,222,226 B2 [issue date, 1 July 2012]). J.J.R. and J.Z. have an issued patent entitled "Cell-specific internalizing RNA aptamers against human CCR5 and used therefor" (USPTO, US 9,605,266 [issue date, 28 March 2017]).

S.S., J.Z., J.C.B., and J.J.R. conceived and designed the experiments. S.S., J.C.B., J.Z., and J.J.R. prepared the animal IACUC protocol, and S.S., J.Z., and J.J.R. wrote the main manuscript and prepared the tables and figures. S.S. and H.L. performed human cell isolation, engraftment, establishment and characterization of hu-NSG mice and HIV-infected hu-NSG mice, and pharmacokinetic profiles analysis of antiretroviral drugs. M.T. helped with isolation of human cells and flow cytometry analysis. S.L. helped with animal engraftment and flow cytometry assay. S.X.W. helped with animal histopathology analysis and H&E staining. T.W.S. helped with pharmacokinetic analysis of antiretroviral drugs and advised on experimental design. J.J.R. and J.C.B. provided funding.

REFERENCES

1. Davey RT, Jr, Bhat N, Yoder C, Chun TW, Metcalf JA, Dewar R, Natarajan V, Lempicki RA, Adelsberger JW, Miller KD, Kovacs JA, Polis MA, Walker RE, Falloon J, Masur H, Gee D, Baseler M, Dimitrov DS, Fauci AS, Lane HC. 1999. HIV-1 and T cell dynamics after interruption of highly active antiretroviral therapy (HAART) in patients with a history of sustained viral suppression. Proc Natl Acad Sci U S A 96:15109–15114. https://doi.org/10.1073/pnas.96.26.15109.
2. Pace MJ, Agosto L, Graf EH, O'Doherty U. 2011. HIV reservoirs and latency models. Virology 411:344–354. https://doi.org/10.1016/j.virol.2010.12.041.
3. Iglesias-Ussel MD, Romerio F. 2011. HIV reservoirs: the new frontier. AIDS Rev 13:13–29.
4. Han Y, Wind-Rotolo M, Yang HC, Siliciano JD, Siliciano RF. 2007. Experimental approaches to the study of HIV-1 latency. Nat Rev Microbiol 5:95–106. https://doi.org/10.1038/nrmicro1580.
5. Van Lint C, Bouchat S, Marcello A. 2013. HIV-1 transcription and latency: an update. Retrovirology 10:67. https://doi.org/10.1186/1742-4690-10-67.
6. Xu L, Zhang Y, Luo G, Li Y. 2015. The roles of stem cell memory T cells in hematological malignancies. J Hematol Oncol 8:113. https://doi.org/10.1186/s13045-015-0214-5.
7. Barton KM, Burch BD, Soriano-Sarabia N, Margolis DM. 2013. Prospects for treatment of latent HIV. Clin Pharmacol Ther 93:46–56. https://doi.org/10.1038/clpt.2012.202.
8. Chun TW, Moir S, Fauci AS. 2015. HIV reservoirs as obstacles and opportunities for an HIV cure. Nat Immunol 16:584–589. https://doi.org/10.1038/ni.3152.
9. Richman DD, Margolis DM, Delaney M, Greene WC, Hazuda D, Pomerantz RJ. 2009. The challenge of finding a cure for HIV infection. Science 323:1304–1307. https://doi.org/10.1126/science.1165706.
10. Marsden MD, Zack JA. 2017. Humanized mouse models for human immunodeficiency virus infection. Annu Rev Virol 4:393–412. https://doi.org/10.1146/annurev-virology-101416-041703.
11. Akkina R, Allam A, Balazs AB, Blankson JN, Burnett JC, Casares S, Garcia JV, Hasenkrug KJ, Kashanchi F, Kitchen SG, Klein F, Kumar P, Luster AD, Poluektova LY, Rao M, Sanders-Beer BE, Shultz LD, Zack JA. 2016. Improvements and limitations of humanized mouse models for HIV research: NIH/NIAID "Meet the Experts" 2015 Workshop Summary. AIDS Res Hum Retroviruses 32:109–119. https://doi.org/10.1089/aid.2015.0258.
12. Akkina R. 2013. New generation humanized mice for virus research: comparative aspects and future prospects. Virology 435:14–28. https://doi.org/10.1016/j.virol.2012.10.007.
13. Ito R, Takahashi T, Katano I, Ito M. 2012. Current advances in humanized mouse models. Cell Mol Immunol 9:208–214. https://doi.org/10.1038/cmi.2012.2.
14. Nehls M, Pfeifer D, Schorpp M, Hedrich H, Boehm T. 1994. New member of the winged-helix protein family disrupted in mouse and rat nude mutations. Nature 372:103–107. https://doi.org/10.1038/372103a0.
15. Bosma GC, Custer RP, Bosma MJ. 1983. A severe combined immunodeficiency mutation in the mouse. Nature 301:527–530. https://doi.org/10.1038/301527a0.
16. Mombaerts P, Iacomini J, Johnson RS, Herrup K, Tonegawa S, Papaioannou VE. 1992. RAG-1-deficient mice have no mature B and T lymphocytes. Cell 68:869–877. https://doi.org/10.1016/0092-8674(92)90030-G.
17. Shinkai Y, Rathbun G, Lam KP, Oltz EM, Stewart V, Mendelsohn M, Charron J, Datta M, Young F, Stall AM, et al. 1992. RAG-2-deficient mice lack mature lymphocytes owing to inability to initiate V(D)J rearrangement. Cell 68:855–867. https://doi.org/10.1016/0092-8674(92)90029-C.
18. Brooks DG, Hamer DH, Arlen PA, Gao L, Bristol G, Kitchen CM, Berger EA, Zack JA. 2003. Molecular characterization, reactivation, and depletion of latent HIV. Immunity 19:413–423. https://doi.org/10.1016/S1074-7613(03)00236-X.
19. Traggiai E, Chicha L, Mazzucchelli L, Bronz L, Piffaretti JC, Lanzavecchia A, Manz MG. 2004. Development of a human adaptive immune system in cord blood cell-transplanted mice. Science 304:104–107. https://doi.org/10.1126/science.1093933.
20. Ishikawa F, Yasukawa M, Lyons B, Yoshida S, Miyamoto T, Yoshimoto G, Watanabe T, Akashi K, Shultz LD, Harada M. 2005. Development of

functional human blood and immune systems in NOD/SCID/IL2 receptor γ chain(null) mice. Blood 106:1565–1573. https://doi.org/10.1182/blood-2005-02-0516.
21. Ohbo K, Suda T, Hashiyama M, Mantani A, Ikebe M, Miyakawa K, Moriyama M, Nakamura M, Katsuki M, Takahashi K, Yamamura K, Sugamura K. 1996. Modulation of hematopoiesis in mice with a truncated mutant of the interleukin-2 receptor gamma chain. Blood 87:956–967.
22. Holt N, Wang J, Kim K, Friedman G, Wang X, Taupin V, Crooks GM, Kohn DB, Gregory PD, Holmes MC, Cannon PM. 2010. Human hematopoietic stem/progenitor cells modified by zinc-finger nucleases targeted to CCR5 control HIV-1 *in vivo*. Nat Biotechnol 28:839–847. https://doi.org/10.1038/nbt.1663.
23. Marsden MD, Kovochich M, Suree N, Shimizu S, Mehta R, Cortado R, Bristol G, An DS, Zack JA. 2012. HIV latency in the humanized BLT mouse. J Virol 86:339–347. https://doi.org/10.1128/JVI.06366-11.
24. Melkus MW, Estes JD, Padgett-Thomas A, Gatlin J, Denton PW, Othieno FA, Wege AK, Haase AT, Garcia JV. 2006. Humanized mice mount specific adaptive and innate immune responses to EBV and TSST-1. Nat Med 12:1316–1322. https://doi.org/10.1038/nm1431.
25. Lan P, Tonomura N, Shimizu A, Wang S, Yang YG. 2006. Reconstitution of a functional human immune system in immunodeficient mice through combined human fetal thymus/liver and CD34$^+$ cell transplantation. Blood 108:487–492. https://doi.org/10.1182/blood-2005-11-4388.
26. Karpel ME, Boutwell CL, Allen TM. 2015. BLT humanized mice as a small animal model of HIV infection. Curr Opin Virol 13:75–80. https://doi.org/10.1016/j.coviro.2015.05.002.
27. Denton PW, Olesen R, Choudhary SK, Archin NM, Wahl A, Swanson MD, Chateau M, Nochi T, Krisko JF, Spagnuolo RA, Margolis DM, Garcia JV. 2012. Generation of HIV latency in humanized BLT mice. J Virol 86:630–634. https://doi.org/10.1128/JVI.06120-11.
28. Zhou J, Satheesan S, Li H, Weinberg MS, Morris KV, Burnett JC, Rossi JJ. 2015. Cell-specific RNA aptamer against human CCR5 specifically targets HIV-1 susceptible cells and inhibits HIV-1 infectivity. Chem Biol 22:379–390. https://doi.org/10.1016/j.chembiol.2015.01.005.
29. Moir S, Fauci AS. 2009. B cells in HIV infection and disease. Nat Rev Immunol 9:235–245. https://doi.org/10.1038/nri2524.
30. Brechtl JR, Breitbart W, Galietta M, Krivo S, Rosenfeld B. 2001. The use of highly active antiretroviral therapy (HAART) in patients with advanced HIV infection: impact on medical, palliative care, and quality of life outcomes. J Pain Symptom Manage 21:41–51. https://doi.org/10.1016/S0885-3924(00)00245-1.
31. Durand CM, Blankson JN, Siliciano RF. 2012. Developing strategies for HIV-1 eradication. Trends Immunol 33:554–562. https://doi.org/10.1016/j.it.2012.07.001.
32. Lu W, Mehraj V, Vyboh K, Cao W, Li T, Routy JP. 2015. CD4:CD8 ratio as a frontier marker for clinical outcome, immune dysfunction and viral reservoir size in virologically suppressed HIV-positive patients. J Int AIDS Soc 18:20052. https://doi.org/10.7448/IAS.18.1.20052.
33. McBride JA, Striker R. 2017. Imbalance in the game of T cells: what can the CD4/CD8 T-cell ratio tell us about HIV and health? PLoS Pathog 13:e1006624. https://doi.org/10.1371/journal.ppat.1006624.
34. Re MC, Vitone F, Biagetti C, Schiavone P, Alessandrini F, Bon I, de Crignis E, Gibellini D. 2010. HIV-1 DNA proviral load in treated and untreated HIV-1 seropositive patients. Clin Microbiol Infect 16:640–646. https://doi.org/10.1111/j.1469-0691.2009.02826.x.
35. Asahchop EL, Meziane O, Mamik MK, Chan WF, Branton WG, Resch L, Gill MJ, Haddad E, Guimond JV, Wainberg MA, Baker GB, Cohen EA, Power C. 2017. Reduced antiretroviral drug efficacy and concentration in HIV-infected microglia contributes to viral persistence in brain. Retrovirology 14:47. https://doi.org/10.1186/s12977-017-0370-5.
36. Reagan-Shaw S, Nihal M, Ahmad N. 2008. Dose translation from animal to human studies revisited. FASEB J 22:659–661. https://doi.org/10.1096/fj.07-9574LSF.
37. Nachman S, Zheng N, Acosta EP, Teppler H, Homony B, Graham B, Fenton T, Xu X, Wenning L, Spector SA, Frenkel LM, Alvero C, Worrell C, Handelsman E, Wiznia A, International Maternal Pediatric Adolescent AIDS Clinical Trials Study Team. 2014. Pharmacokinetics, safety, and 48-week efficacy of oral raltegravir in HIV-1-infected children aged 2 through 18 years. Clin Infect Dis 58:413–422. https://doi.org/10.1093/cid/cit696.
38. Serrao E, Odde S, Ramkumar K, Neamati N. 2009. Raltegravir, elvitegravir, and metoogravir: the birth of "me-too" HIV-1 integrase inhibitors. Retrovirology 6:25. https://doi.org/10.1186/1742-4690-6-25.
39. Barditch-Crovo P, Deeks SG, Collier A, Safrin S, Coakley DF, Miller M, Kearney BP, Coleman RL, Lamy PD, Kahn JO, McGowan I, Lietman PS. 2001. Phase i/ii trial of the pharmacokinetics, safety, and antiretroviral activity of tenofovir disoproxil fumarate in human immunodeficiency virus-infected adults. Antimicrob Agents Chemother 45:2733–2739. https://doi.org/10.1128/AAC.45.10.2733-2739.2001.
40. Wang LH, Wiznia AA, Rathore MH, Chittick GE, Bakshi SS, Emmanuel PJ, Flynn PM. 2004. Pharmacokinetics and safety of single oral doses of emtricitabine in human immunodeficiency virus-infected children. Antimicrob Agents Chemother 48:183–191. https://doi.org/10.1128/AAC.48.1.183-191.2004.
41. Valade E, Treluyer JM, Bouazza N, Ghosn J, Foissac F, Benaboud S, Fauchet F, Viard JP, Urien S, Hirt D. 2014. Population pharmacokinetics of emtricitabine in HIV-1-infected adult patients. Antimicrob Agents Chemother 58:2256–2261. https://doi.org/10.1128/AAC.02058-13.
42. Soldin OP, Mattison DR. 2009. Sex differences in pharmacokinetics and pharmacodynamics. Clin Pharmacokinet 48:143–157. https://doi.org/10.2165/00003088-200948030-00001.
43. Umeh OC, Currier JS. 2006. Sex differences in pharmacokinetics and toxicity of antiretroviral therapy. Expert Opin Drug Metab Toxicol 2:273–283. https://doi.org/10.1517/17425255.2.2.273.
44. Redel L, Le Douce V, Cherrier T, Marban C, Janossy A, Aunis D, Van Lint C, Rohr O, Schwartz C. 2010. HIV-1 regulation of latency in the monocyte-macrophage lineage and in CD4$^+$ T lymphocytes. J Leukoc Biol 87:575–588. https://doi.org/10.1189/jlb.0409264.
45. Deeks SG. 2012. HIV: shock and kill. Nature 487:439–440. https://doi.org/10.1038/487439a.
46. Shang HT, Ding JW, Yu SY, Wu T, Zhang QL, Liang FJ. 2015. Progress and challenges in the use of latent HIV-1 reactivating agents. Acta Pharmacol Sin 36:908–916. https://doi.org/10.1038/aps.2015.22.
47. Laird GM, Eisele EE, Rabi SA, Lai J, Chioma S, Blankson JN, Siliciano JD, Siliciano RF. 2013. Rapid quantification of the latent reservoir for HIV-1 using a viral outgrowth assay. PLoS Pathog 9:e1003398. https://doi.org/10.1371/journal.ppat.1003398.
48. Siliciano JD, Siliciano RF. 2005. Enhanced culture assay for detection and quantitation of latently infected, resting CD4$^+$ T-cells carrying replication-competent virus in HIV-1-infected individuals. Methods Mol Biol 304:3–15.
49. Alcantar-Orozco EM, Gornall H, Baldan V, Hawkins RE, Gilham DE. 2013. Potential limitations of the NSG humanized mouse as a model system to optimize engineered human T cell therapy for cancer. Hum Gene Ther Methods 24:310–320. https://doi.org/10.1089/hgtb.2013.022.
50. Thomas T, Seay K, Zheng JH, Zhang C, Ochsenbauer C, Kappes JC, Goldstein H. 2016. High-throughput humanized mouse models for evaluation of HIV-1 therapeutics and pathogenesis. Methods Mol Biol 1354:221–235. https://doi.org/10.1007/978-1-4939-3046-3_15.
51. Denton PW, Estes JD, Sun Z, Othieno FA, Wei BL, Wege AK, Powell DA, Payne D, Haase AT, Garcia JV. 2008. Antiretroviral pre-exposure prophylaxis prevents vaginal transmission of HIV-1 in humanized BLT mice. PLoS Med 5:e16. https://doi.org/10.1371/journal.pmed.0050016.
52. Denton PW, Krisko JF, Powell DA, Mathias M, Kwak YT, Martinez-Torres F, Zou W, Payne DA, Estes JD, Garcia JV. 2010. Systemic administration of antiretrovirals prior to exposure prevents rectal and intravenous HIV-1 transmission in humanized BLT mice. PLoS One 5:e8829. https://doi.org/10.1371/journal.pone.0008829.
53. Whitney JB, Hill AL, Sanisetty S, Penaloza-MacMaster P, Liu J, Shetty M, Parenteau L, Cabral C, Shields J, Blackmore S, Smith JY, Brinkman AL, Peter LE, Mathew SI, Smith KM, Borducchi EN, Rosenbloom DI, Lewis MG, Hattersley J, Li B, Hesselgesser J, Geleziunas R, Robb ML, Kim JH, Michael NL, Barouch DH. 2014. Rapid seeding of the viral reservoir prior to SIV viraemia in rhesus monkeys. Nature 512:74–77. https://doi.org/10.1038/nature13594.
54. Choudhary SK, Archin NM, Cheema M, Dahl NP, Garcia JV, Margolis DM. 2012. Latent HIV-1 infection of resting CD4$^+$ T cells in the humanized Rag2$^{-/-}$ γc$^{-/-}$ mouse. J Virol 86:114–120. https://doi.org/10.1128/JVI.05590-11.
55. Shanmugasundaram U, Kovarova M, Ho PT, Schramm N, Wahl A, Parniak MA, Garcia JV. 2016. Efficient inhibition of HIV replication in the gastrointestinal and female reproductive tracts of humanized BLT mice by EFdA. PLoS One 11:e0159517. https://doi.org/10.1371/journal.pone.0159517.
56. Veselinovic M, Yang KH, Sykes C, Remling-Mulder L, Kashuba AD, Akkina R. 2016. Mucosal tissue pharmacokinetics of the integrase inhibitor raltegravir in a humanized mouse model: implications for HIV pre-

exposure prophylaxis. Virology 489:173–178. https://doi.org/10.1016/j.virol.2015.12.014.
57. Stoddart CA, Galkina SA, Joshi P, Kosikova G, Moreno ME, Rivera JM, Sloan B, Reeve AB, Sarafianos SG, Murphey-Corb M, Parniak MA. 2015. Oral administration of the nucleoside EFdA (4′-ethynyl-2-fluoro-2′-deoxyadenosine) provides rapid suppression of HIV viremia in humanized mice and favorable pharmacokinetic properties in mice and the rhesus macaque. Antimicrob Agents Chemother 59:4190–4198. https://doi.org/10.1128/AAC.05036-14.
58. Stohr W, Fidler S, McClure M, Weber J, Cooper D, Ramjee G, Kaleebu P, Tambussi G, Schechter M, Babiker A, Phillips RE, Porter K, Frater J. 2013. Duration of HIV-1 viral suppression on cessation of antiretroviral therapy in primary infection correlates with time on therapy. PLoS One 8:e78287. https://doi.org/10.1371/journal.pone.0078287.
59. Gray LR, Roche M, Flynn JK, Wesselingh SL, Gorry PR, Churchill MJ. 2014. Is the central nervous system a reservoir of HIV-1? Curr Opin HIV AIDS 9:552–558. https://doi.org/10.1097/COH.0000000000000108.
60. Chavez L, Calvanese V, Verdin E. 2015. HIV latency is established directly and early in both resting and activated primary CD4 T cells. PLoS Pathog 11:e1004955. https://doi.org/10.1371/journal.ppat.1004955.